TU Delft OPEN

Multi-objective railway timetabling including energy-efficient train trajectory optimization

Gerben M. Scheepmaker[1]
Department of Performance Management and Innovation, Netherlands Railways, the Netherlands.
Department of Transport and Planning, Delft University of Technology, the Netherlands.

Rob M.P. Goverde[2]
Department of Transport and Planning, Delft University of Technology, the Netherlands.

Energy-efficient train driving is an important topic to railway undertakings (RUs) for sustainability and cost reduction. The timetable affects the possibilities for energy-efficient train driving by the amount of running time supplements, which is the topic of energy-efficient train timetabling (EETT). The scientific literature on EETT focuses mainly on the balance between total running time and energy consumption. However, in practice RUs consider a trade-off between the total running time, the infrastructure occupation and the timetable robustness, while energy efficiency is not considered. In this paper we consider a multiple-objective timetabling problem at a microscopic infrastructure level that adds energy consumption to the other three objectives. We approach the multiple-objective problem by a brute force search algorithm, where we use two different methods to compute the optimal solution: a weighted sum method and a distance metric method. We apply the method to a Dutch case study on the corridor between the stations Arnhem Central and Nijmegen with alternating Intercity and Sprinter trains, without intermediate overtaking possibilities. The results indicate that there is a balancing relationship between the total running time and energy consumption, without influencing the infrastructure occupation and robustness. The results of the 10 Pareto-optimal solutions show a variation of 5% for the total running time, 18% for the energy consumption, 0.3% for the extended cycle time, and 0.8% for the buffer time. The shortest running time leads to 18% more energy consumption than the longest running time with 5% more running time supplement. In both cases the extended cycle time and buffer time are almost constant. On the other hand, reducing the infrastructure occupation leads to homogenization of the timetable. Therefore, including energy consumption in the multiple-objective can be used to balance the trade-off between total running time and capacity consumption.

[1] A: Department of Performance Management and Innovation, Netherlands Railways, P.O. Box 2025, 3500 HA Utrecht, the Netherlands. Department of Transport and Planning, Delft University of Technology, P.O. Box 5048, 2600 GA Delft, the Netherlands. E: g.m.scheepmaker@tudelft.nl
[2] A: Department of Transport and Planning, Delft University of Technology, P.O. Box 5048, 2600 GA Delft, the Netherlands. E: r.m.p.goverde@tudelft.nl

1. Introduction

Railway undertaking (RUs) try to minimize their energy consumption in order to reduce the CO_2 emissions as well as to save money. One of the methods to reduce the energy consumption is to apply an energy-efficient driving strategy by the train driver. Therefore, most literature is focused on the optimization of driving strategies or determining algorithms for driver advisory systems (DASs) (Panou et al., 2013) or automatic train operation (ATO) (Yin et al., 2017). A stream of research is focused on the *energy-efficient train control* (*EETC*) driving strategy that minimizes the total traction energy consumption of a train, see Yang et al. (2016) and Scheepmaker et al. (2017) for overviews on this topic. However, the possibilities for the train to apply the EETC driving strategy depend on the running time supplements in the timetable (Scheepmaker and Goverde, 2015). Therefore, another stream of research is focused on the topic of *energy-efficient train timetabling* (*EETT*), that aims to incorporate the EETC driving strategy into the timetable design (Scheepmaker et al., 2017). Research on EETT can be classified into two groups: the first group is focused on synchronizing accelerating and regenerative braking trains, while the second group is focused to determine the optimal amount and distribution of the running time supplements. Regenerative braking can be applied by modern electric trains in which the train uses the engine to brake (generator) and to convert kinetic energy into electricity. This electricity can be fed back over the catenary to surrounding accelerating trains. Examples of research on synchronization of accelerating and regenerative braking trains can be found in Albrecht (2004), Peña-Alcaraz et al. (2012), Li and Lo (2014a,b), Yang et al. (2014), Luan et al. (2018a,b), and Zhou et al. (2018). However, detailed modelling of the power supply system over the catenary should be considered (Scheepmaker and Goverde, 2020), which requires detailed simulation (Stephan, 2008; Arboleya et al., 2020). In this paper we focus on the second group of research about the optimal amount and distribution of the running time supplements. For more details about EETT we refer to the literature review papers of Yang et al. (2016) and Scheepmaker et al. (2017). Scheepmaker et al. (2017) also showed another clustering of papers into two groups based on the type of optimization problem. A first group is focused on the a single objective optimization problem of minimizing the total energy consumption by varying the running time supplements between stops, e.g. Ding et al. (2011), Sicre et al. (2010), Su et al. (2013, 2014), and Scheepmaker and Goverde (2015). Other research considers multiple objective optimization by including the total running time and/or the delays, e.g. Cucala et al. (2012), Yang et al. (2012), Binder and Albrecht (2013), and Wang and Goverde (2016). Below we address the most recent studies on the topic of EETT that are published after Scheepmaker et al. (2017). A summary of the literature review for energy-efficient train timetabling can be found in Table 1.

Part of the current research aims to find the optimal distribution of the running time supplements for a single train over multiple stops and considers a single objective to minimize total energy consumption. Howlett (2016) proved that the optimal control over multiple stops for the EETC leads to the same cruising speed between each two stops. In addition, Scheepmaker et al. (2020a) found that the shorter the distance between stops, the higher the relative running time supplement.

Another part of the current research is focused on EETT for multiple trains in a railway corridor while considering a single objective. Yang et al. (2018) investigated energy-efficient train timetabling for a complete metro line considering the minimization of the total energy consumption including regenerative braking. Although they consider a single-objective optimization problem,

EJTIR 21(4), 2021, pp.1-42
Scheepmaker and Goverde
Multi-objective railway timetabling including energy-efficient train trajectory optimization

3

Table 1: Summary of EETT literature.

Publication	Area	RB	Conflict	Objective(s)				
				TRT	Robust	Cap	Energy	PWT
Albrecht (2004)	C	x	H				x	
Peña-Alcaraz et al. (2012)	C	x	H				x	
Yang et al. (2014)	C	x	H				x	x
Li and Lo (2014a,b)	C	x	H				x	
Zhou et al. (2018)	C	x	H				x	
Luan et al. (2018a,b)	C	x	B		x		x	
Yang et al. (2018)	C	x	H				x	
Su et al. (2020)	C	x	H				x	
Sicre et al. (2010)	S		-				x	
Ding et al. (2011)	S		-				x	
Su et al. (2013)	S		-				x	
Su et al. (2014)	C		H				x	
Scheepmaker and Goverde (2015)	S		-				x	
Howlett (2016)	S		-				x	
Albrecht et al. (2020)	T		B				x	
Scheepmaker et al. (2020a)	S		-				x	
Cucala et al. (2012)	S		-		x		x	
Binder and Albrecht (2013)	S		-		x		x	
Goverde et al. (2016)	N		B	x	x	x	x	x
Wang and Goverde (2017)	C		H		x		x	
Wang and Goverde (2019)	C		H				x	
Yang et al. (2019)	C		H		x		x	x
Xu et al. (2020)	C		H	x			x	
This paper	C		B	x	x	x	x	

Legend: RB = Regenerative Braking, Conflict = conflict detection, TRT = total running time, Robust = robustness/delays, Cap = capacity utilization, PWT = passenger waiting, time, S = single train, T = two trains, C = corridor/line, N = network, H = headway times, B = blocking time.

they include other objectives related to passenger service and cost of the operator. They did this by taking into account constraints for the cycle time and a time window for the total running time with a buffer time between trains. The speed limits are divided into multiple-phases based on the discrete data of the speed limit and they consider a flat track. Su et al. (2020) also considered the topic of EETT for a complete metro line in both directions and aimed to minimize the total energy consumption. The energy consumption includes the usage of regenerative braking energy by synchronizing the accelerating and regenerative trains near stations in the same power supply area. They developed an iterative integrated approach to compute the energy-optimal timetable. First, the energy-efficient driving strategies are computed with a given total running time using a Dynamic Programming algorithm. Second, a Simulated Annealing heuristic algorithm is used to compute the optimal amount of running time and the headway between trains given the scheduled cycle time and the number of trains in the network, while minimizing the total energy consumption of all trains. The algorithm computes the headway based on the passenger demand at all stations. Constraints are included to guarantee the minimum turn back time at the final stations, the maximum running time between stops, the minimum headway between trains, and the minimum dwell time at stations. Albrecht et al. (2020) considered the topic of EETT for two successive trains on a flat track. The authors define a theoretical framework for the optimal driving strategies of two following trains considering safe-separation constraints that aims to minimize the total energy consumption of both trains given a total running time for both trains, while maintaining a safe separation between the trains. Safe separation means that the leading train must leave each signal point

EJTIR 21(4), 2021, pp.1-42
Scheepmaker and Goverde
Multi-objective railway timetabling including energy-efficient train trajectory optimization

4

segment before the following train enters that segment. The authors use the Least Action Clearance Time Algorithm (LACTA) to compute the energy-optimal driving strategy for two following trains given a total amount of running time. Basically, LACTA starts by considering a basic separation in time between trains. LACTA then checks for each time overlap of block section, i.e., whether the leading train left a block section before the following train enters that section. Afterwards, a greedy algorithm includes an additional clearance time constraint for the block section with the biggest time violation and computes the new optimal driving strategies of both trains which is then checked again on the violations. This leads to an iterative process.

Current research on multiple-objective optimization for EETT considers the objectives of total travel time, passenger waiting time, and robustness. Yang et al. (2019) focused on the topic of energy-efficient train timetabling by minimizing the energy consumption, passenger waiting time and robustness. Their definition of robustness is different compared to current literature on timetabling, because they are focused on minimizing the effect of perturbations on the energy consumption and passenger waiting time at the stations instead of train delay. They also included the effect of regenerative braking by maximizing the overlap between accelerating and regenerative braking trains. They considered a random dwell time at intermediate stations of the Beijing metro line and used a non-dominated sorting genetic algorithm II to solve the problem and to find the equally optimal solutions (Pareto front). Train separation was considered by headway times and they considered a heuristic method to determine the energy-efficient driving strategy. Xu et al. (2020) considered the topic of EETT by minimizing the total travel time and energy consumption for high-speed trains in a corridor. They included dynamic headway times between trains in order to shorten the travel times compared to fixed headway times. The minimum headway between two trains was determined using an iterative approach by increasing the headway time by one minute if safety space headway was not met. In order to decrease the computation time, they simplified the problem by excluding coasting, varying gradients, and speed limits.

In practice the aim of RUs for timetable design is mainly on other objectives than energy minimization, such as minimizing the total running time, maximizing the capacity utilization and maximizing the robustness of the timetable. The topic of multiple-objective optimization for timetabling (mainly without considering the objective of minimizing the energy consumption) is intensively studied in literature, see the surveys in Caprara et al. (2007), Lusby et al. (2011), and Cacchiani and Toth (2012). Research in timetable optimization can be separated into aperiodic and periodic timetables. In aperiodic timetables the timetable and number of trains is demand driven providing flexibility, while a periodic timetable provides the same service pattern each period (regularity) (Yan and Goverde, 2019). In this paper our focus is on periodic timetables. Another difference in timetable optimization is the level of details of the infrastructure data. At a macroscopic level the nodes and link model contains aggregate information of the infrastructure (i.e. nodes are stations and links are the complete railway lines between stations), while at a *microscopic level* the nodes and links contain the highest detail information of the infrastructure (i.e. signals, switches, and track sections) (Radtke, 2014). This also leads to a different methodology for conflict detection: in the macroscopic model headway constraints are considered, while in the microscopic model conflicts are detected based on the block section occupation of trains (i.e. only one train can reserve a section of track between adjacent signals). A standard model for representing macroscopic periodic timetable optimization is based on the Periodic Event Scheduling Problem (PESP) (Serafini and Ukovich, 1989; Kroon et al., 2014). A detailed literature review about macroscopic timetable

optimization can be found in Cacchiani and Toth (2012). Research on microscopic timetable optimization is limited (Cacchiani et al., 2014, 2015), because the size of the model increases for the decision variables and constraints when more details are included (Zhang et al., 2019). In addition, multiple-objective timetable optimization research focusing on microscopic timetable optimization including the objective of energy minimization is limited, and is discussed below.

Goverde et al. (2016) considered a three-level iterative framework for timetable design and timetable evaluation which they applied to a Dutch railway network. First, at a macroscopic level they considered a multiple-objective optimization using an Integer Linear programming formulation that minimizes the total running time and dwell time, missed connections, the time of exceeding the nominal transfer time, and cancelled train path requests (i.e. aiming at efficiency). After generating the macroscopic timetable, a delay propagation algorithm is used in order to evaluate the robustness of the macroscopic timetable using a Monte Carlo simulation (Bešinović et al., 2016). Second, at a microscopic level they detect and resolve path of conflicts, and maximize the infrastructure occupation and stability of the timetable (i.e. aiming at feasibility and stability). The model iteratively applies the macro-micro model in order to find a conflict-free, stable and robust timetable that minimizes the objectives on the macroscopic level. Details of this macro-micro interaction can be found in Bešinović et al. (2016). Finally, a mesoscopic fine tuning model is used given the solution from the iterations of the macro-micro model on a corridor level. This mesoscopic model computes the energy-efficient speed profiles considering stochastic dwell time distributions on intermediate stops in order to determine robust energy-efficient speed profiles (i.e. aiming at energy efficiency and robustness). Therefore, energy-efficient train control was considered sequential in the optimization process (after the other objectives). Details about the mesoscopic fine tuning model can be found in the paper of Binder and Albrecht (2013). Wang and Goverde (2017) minimized the total energy consumption and the delays for multiple trains on single-track lines with meeting stations using headway norms. Wang and Goverde (2019) extended this approach to re-allocate the running time supplements in a timetable to optimize the joint energy-efficient speed profiles on general railway networks. They used headway norms during the optimization in order to derive a conflict-free timetable, while they checked the feasibility of the optimal timetable afterwards by using the blocking time stairways.

Based on the literature review it can be concluded that research about energy-efficient train timetabling with multiple-objectives is mainly focused on finding the balance between robustness and energy consumption, see Table 1. However, in practice the primary objectives for RUs are on minimizing the total running time and maximizing the capacity utilization (i.e., frequencies) and robustness, while energy consumption is at best secondary. In addition, Table 1 shows that most research on EETT considers macroscopic timetable feasibility based on normative minimum headway times, while microscopic conflict detection considering the signaling system must be used to guarantee conflict-free timetables in practice (especially closer to the day of operation in order to deliver a realistic and realizable timetable for operation). Only Goverde et al. (2016) considered the multiple objectives of minimizing total running time, robustness, capacity utilization and energy consumption with microscopic conflict detection. However, the objective of energy consumption was considered after a conflict-free, stable and robust timetable structure was determined. Thus, research is missing on simultaneously solving the multiple-objective optimization problem regarding the total running time, capacity utilization using blocking time theory, robustness and energy consumption. In this paper we include the objective of energy consumption upfront as one of the

objectives to minimize (jointly). Therefore, the aim of this paper is to determine the relationship between the total running time, infrastructure occupation, robustness and energy consumption of trains on a corridor. Specifically, we consider a multiple-objective timetabling problem that aims at a trade-off between minimizing the total running time, extended cycle time, energy consumption and maximizing the buffer time at a microscopic level using the blocking times for conflict detection (blocking time theory). Here, we define the *extended cycle time* as the cycle time including a minimum buffer time between trains. We define the cycle time as the minimum interval that a departure order of successive trains in the same direction repeats itself. Therefore, the paper gives the following contributions to the literature:

1. We propose the extended cycle time that includes a minimum buffer time.

2. We consider the multiple-objective optimization problem of minimizing total travel time, extended cycle time and energy consumption, and maximizing the buffer time.

3. We find relationships between energy minimization in relation to the other objectives, specifically between energy consumption and capacity consumption, and between energy consumption and robustness.

4. We focus on microscopic timetable optimization using blocking time theory to develop a conflict-free timetable on a railway corridor.

The structure of the paper is as follows. We first describe the theory regarding the optimal control, blocking time, capacity consumption and robustness in Section 2. This leads to the multiple-objective optimization problem formulation regarding the objectives of total running time, extended cycle time, total buffer time and total traction energy consumption. Section 3 discusses the method used to compute the optimal solution. Afterwards, we consider a real-world case to investigate the balance between the multiple objectives in Section 4. Finally, Section 5 discusses the main conclusions of this paper.

2. Theory

This section discusses the theoretical background that is used in the method to tackle the multiple-objective problem. In Section 2.1 the optimal control problem is discussed that leads to the optimal driving strategies that are the foundation of our method to compute the optimal timetable. In addition, the optimal control leads to the objectives of minimizing total energy consumption and total running time. Section 2.2 discusses the blocking time theory that is used in order to derive a conflict-free timetable on a railway corridor for multiple following trains. Afterwards, Section 2.3 discusses the UIC 406 method of timetable compression in order to derive the capacity consumption and extended cycle time of a timetable, which is one of the objectives to optimize. Finally, the fourth objective in our paper is to maximize the robustness of the timetable by maximizing the total buffer time. Therefore, the topic of timetable robustness is discussed in Section 2.4.

EJTIR 21(4), 2021, pp.1-42
Scheepmaker and Goverde
Multi-objective railway timetabling including energy-efficient train trajectory optimization

7

2.1 Optimal train control

In this section we discuss the optimal train control problems in order to derive the two driving strategies considered in this paper: the energy-efficient train control (EETC) and the minimum time train control (MTTC). We consider mechanical braking only and we model the train as a point mass (Brünger and Dahlhaus, 2014; Howlett and Pudney, 1995). The derivation of the EETC and MTTC optimal control structure between two consecutive stops by using distance as independent variable is discussed in Scheepmaker et al. (2020a). Therefore, in this paper we only provide the optimal control problem formulation and briefly discuss the different driving regimes for the optimal driving strategies. Section 2.1.1 discusses the EETC problem formulation and in Section 2.1.2 the MTTC problem formulation is discussed.

Energy-Efficient Train Control

The EETC driving strategy aims to minimize total traction energy consumption Z_E [m^2/s^2] over a railway line with total distance S [m] and $l-1$ sections over stop positions $(s_0, \ldots, s_l)$ with a total scheduled running time T [s]:

$$Z_E = \min \int_{s_0}^{s_l} f(s)ds, \tag{1}$$

subject to the constraints

$$\dot{t}(s) = \frac{1}{v(s)} \tag{2}$$

$$\dot{v}(s) = \frac{f(s) + b(s) - r(v) - g(s)}{v(s)} \tag{3}$$

$$0 \leq v(s) \leq v_{\max}(s) \tag{4}$$

$$f(s)v(s) \leq p_{\max} \tag{5}$$

$$0 \leq f(s) \leq f_{\max} \tag{6}$$

$$-b_{\min} \leq b(s) \leq 0 \tag{7}$$

$$t(s_0) = 0, \ t(s_l) = T \tag{8}$$

$$v(s_i) = 0, \ \text{for } i = 1, \ldots, l, \tag{9}$$

where distance s [m] is the independent variable, time t [s] and speed v [m/s] are the state variables. Eqs. (2) and (3) are the dynamic equations describing the derivatives of the state variables to the independent variable s, i.e. $\dot{t} = dt/ds$ and $\dot{v} = dv/ds$. Eq. (4)–(7) describe the path constraints. The control variables are the mass-specific traction f [m/s^2] and mass-specific mechanical braking b [m/s^2]. The mass-specific forces are computed by dividing the total force force F [N] over the total rotating mass ρm (rotating mass factor ρ [-] multiplied by the train mass m [kg]), i.e., $F(t)/(\rho m)$. The mass-specific traction force f (see Eq. (6)) is bounded between zero and the minimum of the

maximum mass-specific traction force and the maximum mass-specific power p [m^2/s^3] divided by the speed (see Eq. (5)), i.e. $f(v) \in [0, \min(f_{\max}, p_{\max}/v)]$. The mass-specific mechanical braking force is bounded between zero and the maximum braking force, i.e. $b(v) \in [-b_{\min}, 0]$, see Eq. (7). Traction and braking control cannot be applied at the same time, i.e., $fb = 0$. Combining the mass-specific train resistance $r(v)$ [m/s^2] and the mass-specific line resistance $g(s)$ [m/s^2] leads to the total mass-specific train resistance. We use the general mass-specific train resistance based on Davis equation $r(v) = r_0 + r_1 v + r_2 v^2$ that consists of non-negative coefficients $r_0, r_1 \geq 0$ and $r_2 > 0$ (Davis, 1926). The mass-specific line resistance is determined by gradients $g(s)$ with $g(s) > 0$ indicating uphill slopes and $g(s) < 0$ downhill slopes. The speed is limited between 0 and the speed limit $v_{\max}$ that depends on distance, see Eq. (4). In this paper a piecewise-constant speed limit and gradient is considered over the complete trajectory. The boundary conditions are described by Eqs. (8) for the time and (9) for the speed. Note that we do not provide time constraints on the intermediate stops, so the optimal arrival and departure times will be determined by the optimization problem. Intermediate event constraints (9) force the speed at stop i at distance s_i to be zero.

Similar to Scheepmaker et al. (2020a) we can define the Hamiltonian, augmented Hamiltonian and costates using the EETC optimal control structure. Pontryagin's Maximum Principle (PMP) gives the optimal controls by maximizing the Hamiltonian, and the necessary optimally conditions are determined by applying the Karush-Kuhn-Tucker (KKT) conditions on the augmented Hamiltonian. Scheepmaker et al. (2020a) showed that the general optimal control structure over multiple stops is similar to the optimal control structure between two successive stops.

In general, the optimal control structure consists of the driving regimes maximum acceleration by maximum traction force, cruising at a constant speed by partial traction/braking (i.e. balance between the traction or braking force and the total train resistance), coasting (zero control), and maximum braking. Note that the optimal cruising speed can be lower than the speed limit. In addition, for short distances between two stops the optimal control structure does not include cruising (Scheepmaker et al., 2017, 2020b).

Minimum Time Train Control

The aim of minimum time train control (MTTC) is to minimize the total running time of the train Z_R [s]:

$$Z_R = \min t(s_l), \tag{10}$$

subject to the constraints (2)–(9), and where here the final time $t(s_l)$ is free and will be minimized. Similar to the EETC problem formulation the Hamiltonian, augmented Hamiltonian and costates can be derived. The PMP and the KKT conditions can be applied on them in order to derive the optimal control structure. The structure consists of the driving regimes maximum acceleration, cruising at the speed limit and maximum braking. The general optimal control structure for the MTTC driving strategy is similar to the optimal control structure between two successive stops (Scheepmaker et al., 2020a).

2.2 Blocking Time Theory

The railway infrastructure is partitioned in different block sections for safe train operation. Each block section is covered by a signal that indicates if the next block section is available for the train approaching the signal. A three-aspect two-block signalling system is assumed, which means that an approach signal in advance indicates if the train needs to brake for the next (stop) signal. The time duration in which a specific block section is allocated to a specific train and thus blocked for other trains is called blocking time. The following components are considered for the blocking times, see Figure 1 (a):

1. Setup time: time to set and lock the route in the block.

2. Sight and reaction time: the time for the train driver to see and anticipate on the approach signal.

3. Approach time: the time for the train to run from the approach signal to the signal at the end of the approaching block section.

4. Running time: the time to run the train through the block section and possible overlap.

5. Clearing time: the time needed for the train to clear the block section over the train length.

6. Release time: the time to release the route in the block. Part of a block section might be released earlier after the full train length passed the clearing point of a switch within a block section according to the sectional release route locking principle.

We refer to Pachl (2009) and Pachl (2014) for more information about the blocking time theory. One of the results of blocking time theory is the timetable compression method that provides the minimum headway between trains of two conflict-free train paths (Bešinović and Goverde, 2018).

In addition, a timetable must include scheduled buffer time between two trains. Buffer time is an empty time slot between two successive trains on top of their minimum headway time (Pachl, 2014). The minimum (line) headway time on a corridor is defined as the minimal conflict-free inter-departure time between two train paths given the speed profiles of the two trains (Pachl, 2014). Buffer times are used to avoid or reduce the propagation of delays to other trains, the so called secondary or knock-on delays (Goverde and Hansen, 2013). In practice, infrastructure managers and RUs consider a minimum buffer time between two trains as a measure to deal with scheduled deviations (also called critical buffer time by Jensen et al. (2017)). Therefore, we define the concept of extended blocking time, which includes a minimum buffer time (see Figure 1 (a)). Plotting successive extended blocking times in a time-distance diagram leads to the extended blocking time stairway, as shown in Figure 1 (b). The extended blocking time stairway gives the extended minimum line headway between two successive trains as can be seen in Figure 1 (b).

Conflicts occur when blocking times of two trains overlap. In addition, buffer time conflicts occur when the required minimum buffer time is overlapping with the blocking time of another train. In this paper we aim at a conflict-free timetable. Detailed information about blocking time theory can be found in Pachl (2009) and Pachl (2014).
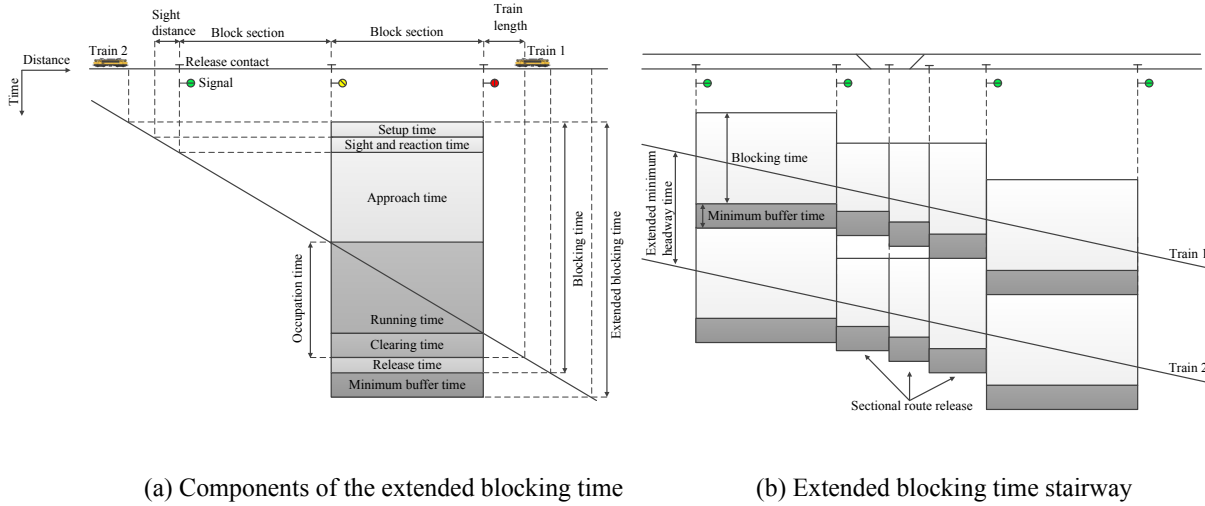
(a) Components of the extended blocking time (b) Extended blocking time stairway

Figure 1: The left plot (a) shows the attributes for the extended blocking time stairway including the minimum buffer time for a three-aspect signalling system. The right plot (b) indicates a partial blocking time stairway for two successive trains including the (minimum) buffer time.

2.3 Capacity Consumption

There are different timetable performance indicators to assess a timetable. One of them is the *infrastructure occupation*, which is defined as the amount of time that the infrastructure is blocked by train paths from a given timetable structure in a given time window (UIC, 2013). This performance indicator provides insight in the potential bottlenecks in a network and is related to the capacity consumption of a corridor. The *capacity consumption* includes the required buffer time between trains on top of the infrastructure occupation (UIC, 2013; Jensen et al., 2017). The infrastructure occupation depends on the infrastructure (route, speed limits, block lengths, and signalling system), the rolling stock characteristics (such as the train composition, acceleration and braking, maximum speed, and length), and timetable (frequencies, heterogeneity, and dwell times) (Goverde and Hansen, 2013; Bešinović and Goverde, 2018). The UIC 406 timetable compression method can be used to compute the infrastructure occupation on a line (UIC, 2013). The location where the blocking stairways of two trains touch each other are the critical block sections. The infrastructure occupation can be extended to extended infrastructure occupation where the extended blocking time stairways, as described in Section 2.2, are compressed, see Figure 2. Note that then the capacity consumption consists of the extended infrastructure occupation plus possible additional buffer time on top of the minimum buffer times. The capacity consumption is analyzed over a certain defined time period, for instance 30 min. The extended infrastructure occupation time t_o [s] is then defined from the start of the first train to the start of the compressed first train of the next time period t_p [s], see Figure 2. The extended infrastructure occupation time t_o is thus computed as the sum of the minimum line headway times t_{ij}^h [s] for the successive trains (Bešinović et al., 2017)

$$t_o = \sum_{(i,j) \in W_p} t_{ij}^h, \tag{11}$$

where W_p is the pattern of successive train pairs (i, j) over the scheduled time period, and t_{ij}^h is the minimum headway time from train i to train j calculated over the corridor with n_b blocks as (Bešinović et al., 2017)

$$t_{ij}^h = \max_{k \in 1,\ldots,n_b} (t_{ik}^e - t_{jk}^b), \tag{12}$$

where t_{ik}^e is the end of the blocking time of train i in block section k including the minimum buffer time, and t_{jk}^b is the begin of the blocking time of train j in block section k. The capacity consumption C_s [%] includes additional scheduled buffer time t_a [s] on top of the minimum buffer time due to e.g. rounding of the timetable to whole minutes or for robustness. This capacity consumption can be computed by

$$C_s = \frac{t_o + t_a}{t_p} \cdot 100\%. \tag{13}$$

We consider a cyclic timetable consisting of one or more train cycles, thus the extended infrastructure occupation time is equal to a multiple of the extended cycle time. Therefore, in order to minimize the infrastructure occupation we can also minimize the extended cycle time instead. The extended cycle time t_c [s] considers the minimum periodic pattern of all trains. In case that all trains have the same frequency f_l, the extended cycle time the cyclic pattern of all train lines can be computed by:

$$t_c = \frac{t_o}{f_l}. \tag{14}$$

Finally, we aim to to minimize the extended cycle time Z_c [s] by

$$Z_c = \min t_c. \tag{15}$$

2.4 Robustness

The topic of robustness in railway planning is considered in the literature review paper of Lusby et al. (2018). They noticed that there is no common definition of robustness for all stakeholders, but that it in general is focused on the capacity for the railway system to function during disturbances (i.e. how the timetable functions during uncertainty by small deviations from train paths). Cacchiani and Toth (2012) also discussed the topic of robustness for timetabling problems. They indicate that robust timetables try to avoid delay propagation in the railway network during disruptions. Goverde and Hansen (2013) define different performance indicators for railway timetables of which one of them is timetable robustness, which are applied in the three-level timetable design framework of
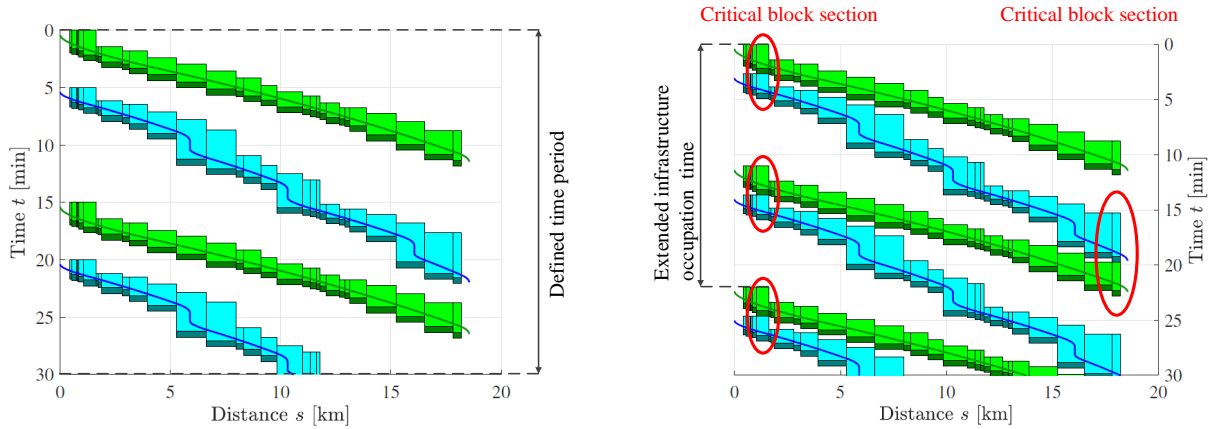
Figure 2: The left plot shows the timetable compression method with timetable before compression. The right plot indicates the timetable compression method with timetable after compression including the minimum buffer time and the critical blocks. Note that the darker area below the blocks indicates the minimum buffer time between trains that are included in the extended blocking times.

Goverde et al. (2016). They consider robustness as the ability of the timetable to cope with design errors, parameter variations, and changing operational conditions, which depend on stochastic processes such as running, dwelling and turning. The aim is to minimize the primary delays (caused by variations in a process that takes longer than the scheduled process time) and secondary or knock-on delays (caused by delays exceeding the scheduled buffer time between two trains at a critical block section) (Vromans et al., 2006; Goverde et al., 2016). Therefore, running time supplements and buffer times between trains are included in order to improve the robustness of the timetable. Running time supplements are the extra running time above the minimum running time in order to minimize primary delays caused by variations of the process times (Goverde et al., 2013; Scheepmaker and Goverde, 2015).

In this paper we consider *the total buffer time* t_b as a measure of the *robustness* of the timetable, which we aim to maximize. The buffer time is also considered in practice for timetable design and evaluation in the Netherlands, where a minimum buffer time (a wake) behind each passenger train is considered for timetable robustness, which is analyzed using a deterministic simulation run. We use a similar approach as considered by NS for timetable robustness. The total buffer time consists of the total minimum buffer time and the additional buffer time. For a cyclic timetable the total buffer time t_b can be computed as:

$$t_b = \frac{T}{f_l} - t_c. \tag{16}$$

Finally, we aim to maximize the robustness of the timetable by maximizing the total buffer time Z_b [s]:

$$Z_b = \max t_b. \tag{17}$$

3. Method

This section discusses the method for the multiple-objective optimization problem. In this paper we apply a brute force algorithm to generate the optimal solutions by considering the running time supplements as a variable for the train and then compute the optimal driving strategy for a single train including the blocking times. We consider a corridor of different train types in a specified time window, and compute the associated total running time as well as the total energy consumption of all trains. Next, we apply the UIC 406 timetable compression method on the corridor in order to determine the extended cycle time and buffer time.

Section 3.1 explains the model PROMO (PseudospectRal Optimal train control MOdel) that is used to compute the different driving strategies and blocking times, that are necessary for the blocking time theory. The brute force search is explained in Section 3.2. In this search we use two methods to compute the optimal solutions.

3.1 PROMO

We used the Radau pseudospectral method to compute the MTTC and EETC driving strategies. In this method orthogonal collocation is applied at the Legendre-Gaus-Radau (LGR) points in order to discretize the optimal control problem. The optimal control problem is then rewritten to a nonlinear programming (NLP) problem that is solved using standard NLP solvers (Betts, 2010). We refer to Wang and Goverde (2016) and Goverde et al. (2021) for more details about the discretization of the optimal control problem and to Garg et al. (2009) and Rao et al. (2010) for general background about the pseudospectral method.

We used the model called PROMO as described in Scheepmaker et al. (2020a) to compute the MTTC and EETC driving strategies. PROMO uses the GPOPS (General Purpose OPtimal Control Software) toolbox of MATLAB, which implements a Radau pseudospectral method to solve the optimal control problem (Rao et al., 2011). We applied PROMO in GPOPS version 4.1 using a laptop with a 2.1 GHz processor and 8 GB RAM. We consider two different train types, an Intercity (IC) or long distance train that stops only at main stations and a Sprinter (SPR) or regional train that stops at all stations. We applied the multiple-phase model of Scheepmaker et al. (2020a) to compute the optimal trajectory for the trains, in which we define a phase between each two stops (i.e., no separate phases for the speed limits and gradients). Each stop needs to be a new phase, because then a collocation point at that stop is guaranteed in GPOPS. The objective is to determine the optimal distribution of the running time supplements over the trajectory in order to minimize the total traction energy consumption over the multiple runs. The model results are verified to see if they are in line with the necessary optimality conditions.

In addition, PROMO computes the extended blocking time for each block section over the trajectory for a single train using the blocking time theory as described in Section 2.2. The computation is done for multiple trains over a corridor. Afterwards, the extended cycle time (and maximum frequency)

over the corridor is computed by applying the UIC 406 compression method as described in Section 2.3. The total buffer time is computed by using Eq. (16). Finally, a balance between different objectives can be determined by comparing the running time, extended cycle time, buffer time and energy consumption for each different combination of running time supplements for the IC and SPR. These combinations are determined by varying the running time supplements of the trains over the corridor.

3.2 Brute force search

In this section we explain the approach of the brute force search algorithm in order to determine the optimal solutions for the single and multiple-objective optimizations. We consider the running time supplements as the main variables in this paper, because they influence all objectives. In general, increasing the running time supplements increases the total running time and decreases the energy consumption. The effect of the running time supplements on the cycle time and buffer time depends on the infrastructure, timetable and rolling stock. Therefore, by adjusting the running time supplements the interaction between the different objectives can be investigated.

The brute force search consist of the following four main steps (see Algorithm 1):

1. Compute the energy-efficient driving strategy for both the IC and SPR for running time supplements ranging from 0% until 15% with a step-size of 0.5% using PROMO. We define x as the total running time of the IC and y as the total running time of the SPR, where the MTTC driving strategy is the reference. PROMO generates the speed profile, energy consumption, as well as the blocking time per train for each given running time. For readability we only show the results of the step-size of 1% in the tables and figures. We define combination xy for each running time supplement combination for an IC-SPR cycle, where m is the total number of running time supplements for the IC and n is the total number of running time supplements for the SPR. Thus in total we have mn combinations of xy IC-SPR cycles.

2. Apply the UIC 406 compression method to compute the minimum extended cycle time for an IC-SPR cycle and the buffer time for all combinations of xy between 0% and 15% running time supplements (step-size of 0.5%) for the IC and SPR.

3. Develop four matrices with the values of the objectives of the total running time Z_R, extended cycle time Z_c, total buffer time Z_b and energy consumption Z_E for each combination of running time supplements (xy) of the IC-SPR cycle. Each entry in the table consists of a combination of the given running time supplement of the IC (columns) and SPR (rows).

4. Compute the optimal solution using two different methods. The first method is the *weighted sum method* in which we minimize the weighted sum given a weight factor for each of the objective functions (Yan and Goverde, 2019). The second method is based on the optimal standardized Euclidean distance (*standard Euclidean distance method*) (Yan et al., 2019). We use these methods because they are most common and relative simple methods, and the weighted sum method considers the importance of the railway undertakings for each single objective by the weight factors.

We start by explaining the weighted sum method. Basically the weighted sum method is a scalarization method which combines all objectives into a single objective (Marler and Arora, 2004). However, when all weights are positive the Pareto optimal solution is achieved by minimizing the weighted sum. Before we can apply the weighted sum method, we need to scale the different objectives with different weight factors in order to compare them (Yan and Goverde, 2019). Since the objectives of total running time, extended cycle time and total buffer time are defined in seconds, we consider this basic scaling to compare the different objectives. We consider the total running time as reference with value 1. We compute the scaling by comparing for each running time supplement combination xy the two objectives with each other with the total average ratio as a scaling factor. This leads to the following scaled formulation of the different single objectives:

$$V_R^{xy} = Z_R^{xy}, \qquad V_c^{xy} = \left(\frac{1}{mn}\sum_{x=1}^{m}\sum_{y=1}^{n}\frac{Z_c^{xy}}{Z_R^{xy}}\right)^{-1} Z_c^{xy}, \qquad V_b^{xy} = \left(\frac{1}{mn}\sum_{x=1}^{m}\sum_{y=1}^{n}\frac{Z_b^{xy}}{Z_R^{xy}}\right)^{-1} Z_b^{xy}. \qquad (18)$$

Since buffer times should be maximized, we rewrite this to minimize the negative value of the buffer time in order to minimize all objectives (i.e. $\max Z_b = -\min Z_b$). In addition, we apply a sensitivity analyses where we see the effect of the optimal solution by varying between the minimum and maximum ratio given the data. Since energy consumption is measured in a complete different unit (kWh), it is difficult to scale this objective with the other objectives that have units in s. Therefore, a scaling factor ω is used and varied using a sensitivity analysis to find a balance between energy consumption and the other objectives:

$$V_E^{xy} = \omega Z_E^{xy}. \qquad (19)$$

The weighted sum (affine combination) with weight factors w_i for $i = 1,...,4$ (for each of the four objectives) and $\sum_{i=1}^{4} w_i = 1$ for the xyth solution can be computed by:

$$\alpha_{xy} = w_1 V_R^{xy} + w_2 V_c^{xy} - w_3 V_b^{xy} + w_4 V_E^{xy}. \qquad (20)$$

A sensitive analysis is applied in order to determine the weight factors, which will be discussed in Section 4.4.1.

Second, we explain the steps to derive the standard Euclidean distance. We first need to standardize the results on the interval $[0,1]$ for each element in the different tables by using the min-max normalization (Yan et al., 2019), i.e., for the objective of running time the normalized objective value is

EJTIR 21(4), 2021, pp.1-42
Scheepmaker and Goverde
Multi-objective railway timetabling including energy-efficient train trajectory optimization

16

$$\tilde{Z}_R^{xy} = \frac{Z_R^{xy} - Z_R^{\min}}{Z_R^{\max} - Z_R^{\min}}, \tag{21}$$

where $Z_R^{\min}$ and $Z_R^{\max}$ are respectively the minimum and maximum over the entire matrix of Z_R. The normalized objective values of the other objectives Z_c and Z_E are computed in the same way. Since the buffer times are to be maximized, we compute first Z_b the same way as Z_R and afterwards we compute the normalized objective value for the buffer time by $\tilde{Z}_b^{xy} = 1 - \tilde{Z}_b^{xy}$, in order to minimize all the objectives. Finally, we determine the optimal standardized Euclidean distance for each combination xy as:

$$\beta_{xy} = \sqrt{(\tilde{Z}_R^{xy})^2 + (\tilde{Z}_c^{xy})^2 + (\tilde{Z}_b^{xy})^2 + (\tilde{Z}_E^{xy})^2}. \tag{22}$$

Algorithm 1: Brute-force search algorithm.

Data: Infrastructure, rolling stock, interlocking, and timetable.
Result: The optimal solutions for the single and multiple-objective optimizations;
Compute MTTC driving strategy for the IC ($x = 1$) and SPR ($y = 1$) ;
for $x = 1.005, 1.010, 1.015, ..., 1.15$ **do**
  Compute EETC driving strategy for the IC with x running time supplement;

for $y = 1.005, 1.010, 1.015, ..., 1.15$ **do**
  Compute EETC driving strategy for the SPR with y running time supplement;

for $x = 1, 1.005, 1.010, ..., 1.15$ **do**
  for $y = 1, 1.005, 1.010, ..., 1.15$ **do**
    Apply UIC 406 compression method for each xy IC-SPR cycle combination;
    Compute Z_R, Z_c, Z_b, and Z_E for each xy IC-SPR cycle combination;

Compute weighted sum method α;
Compute standard Euclidean distance method β;

---

4. Case Study

In this section we apply our model on different scenarios in a case study in order to find a balance between the objectives of minimizing total travel time for the passengers, extended cycle, and energy consumption as well as maximizing the buffer time for robustness. We start by providing the input of the case study, see Section 4.1. In Section 4.2 we discuss the results for the different single objectives. We make a comparison between the different objectives in Section 4.3. Afterwards, we consider the optimization of the multiple objectives in Section 4.4. We analyze the effect of varying the minimum buffer time on the multiple objectives in Section 4.5. Finally, a discussion of the main results is presented in Section 4.6.

4.1 Case study description

The case study considers the railway line between the main stations Arnhem Central (Ah) and Nijmegen (Nm) in the Netherlands with the intermediate stations Arnhem South (Ahz), Elst (Est) and Nijmegen Lent (Nml). The detailed track layout of this railway line can be seen in Figure 3 and the details in one direction about the location of the gradients, speed limits and signals can be found in Table 6 in Appendix A, which is based on the infrastructure data from ProRail (ProRail, 2020). The trains are running over the right-hand tracks for the double track sections. We consider two different electrified train types operating on this network: an Intercity (IC) or long distance train only stopping at the main stations Ah and Nm, and a Sprinter (SPR) or regional train stopping at all stations. The IC and SPR share the same route over the infrastructure, except at the first and last block section due to different track and platform use at Ah and Nm (i.e. we do not consider overtaking on the open track between these stations). We set the maximum passenger comfort braking to 0.5 m/s^2, according to practice in the timetable design at the Netherlands Railways (NS). The trains receive their electricity from the 1.5 kV DC catenary system. We develop microscopic conflict-free timetables using the blocking time theory as described in Section 2.2, therefore, we assume that there is only a red signal approach at the final platform signal at Nm. The general characteristics and parameter setting times can be found in Appendix A in Table 7 and 8 that are partially adopted from Goverde et al. (2013) and Scheepmaker et al. (2020b).

The Dutch timetable is cyclic and in general repeats itself every half hour. In the current Dutch timetable trains operate with frequencies of at least two trains per hour. Therefore, we use a half hour time interval. We consider the running time supplements and the minimum buffer time between trains as basic measures for timetable robustness. In the Netherlands the current minimum buffer time is 60 s. However, the aim is to reduce this buffer time to 30 s by for instance using ATO in order to increase the number of trains in the network without expensive infrastructure cost. In this paper we set the minimum buffer time to 30 s, but we also investigate the effect of increasing the minimum buffer time to 60 s. The minimum extended cycle time is computed using the UIC 406 compression method as described in Section 2.3. Finally, we consider an increase in the frequency of the IC-SPR train when this is enabled by the extended cycle time, because this leads to a higher service to the passengers. For instance an extended cycle time of 720 s leads to 4 IC-SPR cycles per hour, while an extended cycle time of 719 s gives 5 IC-SPR cycles per hour. However, the increase in the frequency of the IC-SPR cycles reduces the total buffer time.

4.2 Results of the indicators

In this section we discuss the results of different indicators where we differentiate between the separate IC and SPR, and the IC-SPR cycle. First, we analyze the separate results of the IC (Figure 4) and SPR (Figure 5) in terms of speed profile and energy consumption. The results of the driving strategies of the IC and SPR with varying running time supplements are shown in Table 9 (Appendix B), while the optimal distribution of the running time supplements over multiple-stops for the SPR is shown in Table 10 (Appendix B).

We start by analyzing the results of the speed-distance and energy-distance profiles of the IC (Figure 4) and SPR (Figure 5), where we varied the amount of running time supplements. Figure 4 indicates for the IC that the higher the amount of running time supplement, the earlier the train starts to coast. With limited running time supplement up to 4% the speed-distance plot indicates two coasting
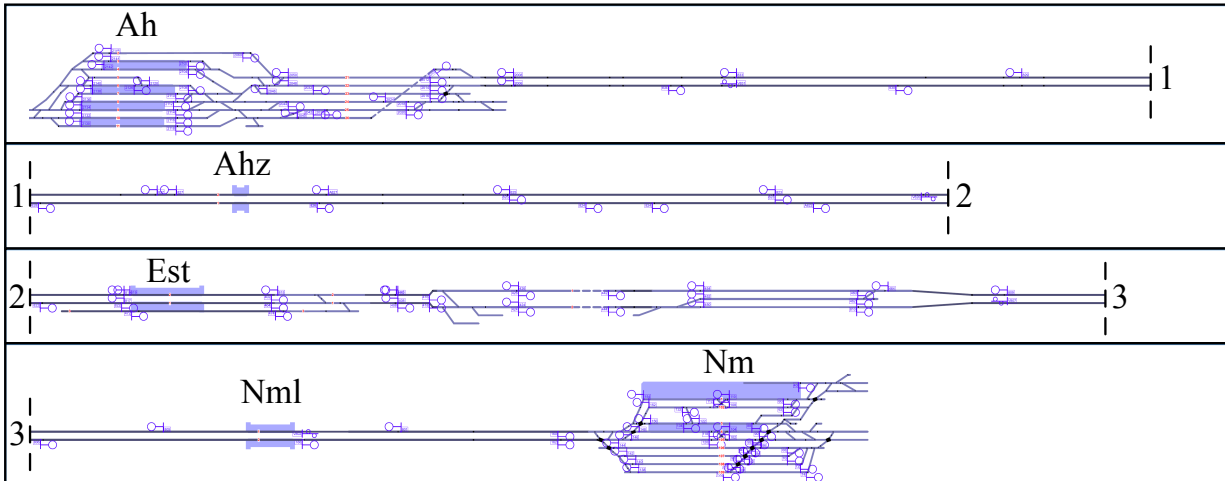
EJTIR 21(4), 2021, pp.1-42
Scheepmaker and Goverde
Multi-objective railway timetabling including energy-efficient train trajectory optimization

18

Figure 3: Detailed track layout of railway line Arnhem Central (Ah)–Nijmegen (Nm).

phases: one before and one after the reduced speed limit of 130 km/h after Est with possibly a short distance of maximum acceleration after the reduced speed limit of 130 km/h before coasting. In case that the running time supplements are at least 10% we see that the optimal driving strategy does not include cruising at the speed limit, but the train starts to coast directly after maximum acceleration. Table 9 indicates that the energy savings of the EETC driving strategy for the IC vary between 24% and 57% compared to the MTTC driving strategy. The resulting speed-distance profile of the SPR is shown in Figure 5. In general, the figure indicates that when there are sufficient running time supplements, the optimal driving regime between each of the stops consists of maximum acceleration, coasting and maximum braking, with a possible cruising regime at the speed limit where the speed limit is reached. The results in Figure 5 and Table 10 also indicate that relatively more running time supplement is included for shorter distance sections where the train can start coasting at relatively lower speeds, which is in line with the results of Scheepmaker et al. (2020a). The exception is at the short section Nml-Nm (2.4 km) that includes a speed limit restriction of 40 km/h. The results indicate that coasting below 70 km/h takes relatively much running time supplement while the energy savings are limited. The energy savings of the SPR by the EETC driving strategy vary between 18% and 56% compared to the MTTC driving strategy (see Table 9).

Afterwards, we continue on the interaction of the trains by analyzing the IC-SPR cycles. We analyze the results of the IC-SPR cycle for the total running time, followed by the extended cycle time and buffer time. Then, we discuss the results of the energy consumption of the IC-SPR cycle. Table 11 (Appendix B) gives the total running time per IC-SPR cycle and the extended cycle time per IC-SPR cycle is shown in Table 12 (Appendix B). Table 13 (Appendix B) gives the buffer time per IC-SPR cycle and the total energy consumption per IC-SPR cycle is provided by Table 14 (Appendix B). The results of the different driving strategies and IC-SPR cycles are also visualized in Figures 6–10.

Table 11 and the contour plot in the left plot of Figure 6 obviously indicate that more running time supplements for the IC and/or SPR leads to a higher total running time. The MTTC driving strategy provides the solution that minimizes total travel time. For the MTTC driving strategy the resulting
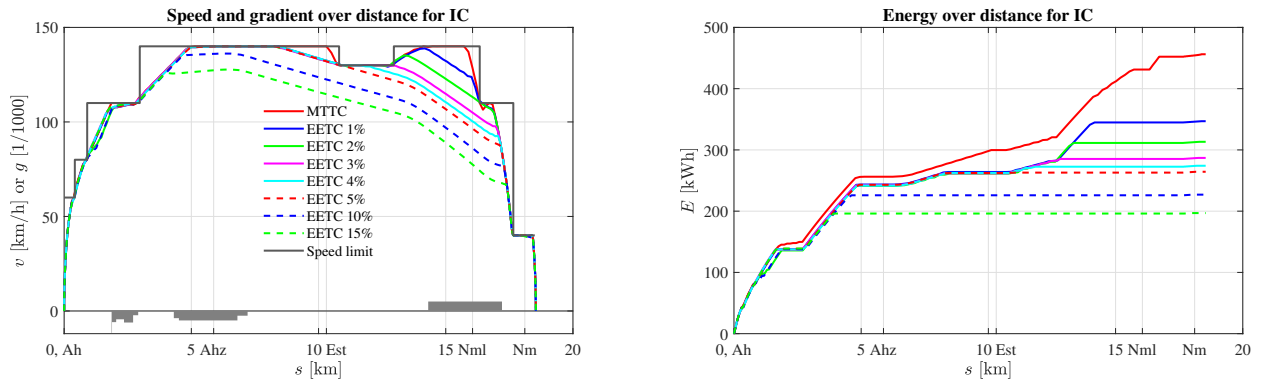
Figure 4: The left plot shows for the case Ah-Nm IC with varying running time supplements the speed/gradient–distance profile of the MTTC and EETC driving strategies. The right plot indicates the energy–distance profile of the MTTC and EETC driving strategies for the case Ah-Nm IC.
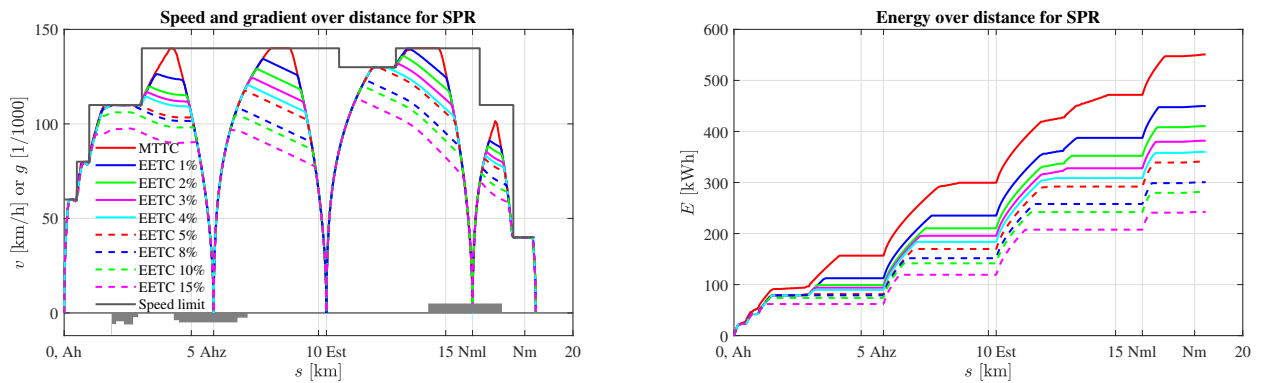
Figure 5: The left plot shows for the case Ah-Nm SPR with varying running time supplements the speed/gradient–distance profile of the MTTC and EETC driving strategies. The right plot indicates the energy–distance profile of the MTTC and EETC driving strategies for the case Ah-Nm SPR.

compressed timetable is shown in the left part of Figure 7, indicating that the critical blocks are block 3 after Ah (IC-SPR) and block 17 at Nm (SPR-IC).

Table 12 shows that more running time supplement for the IC leads to a lower extended cycle time, while including more running time supplement for the SPR increases the extended cycle time. This effect can also be seen in the contour plot of the total extended cycle time in the left plot in Figure 8. The contour plot shows that the curves with low values of the extended cycle times (i.e. 640 s and 660 s) intersect the vertical axis of the varying running time (supplements) of the IC, indicating that with 0% running time supplements for the SPR and high amount of running time supplements of the IC, the smallest extended cycle time can be achieved. The resulting compressed timetable of the driving scenario with 15% running time supplements for the IC and 0% for the SPR is shown in the left part of Figure 9, indicating that block 7 at Ahz (IC-SPR) and block 17 at Nm (SPR-IC) are the critical blocks. Lower extended cycle times enable higher frequencies of the IC-SPR train cycles. The results are in line with common knowledge in practice that homogenization leads to a

Figure 6: The left plot shows the contour plot for the case Ah-Nm for the total cycle running time over the total running time (supplements) for the SPR and IC. The right plot indicates the Pareto frontier curve of the energy consumption over the total running time for the IC and SPR for the case Ah-Nm.

Figure 7: The left plot shows for the case Ah-Nm for the IC (green) and SPR (blue) compressed blocking time diagram of the MTTC driving strategies. The right plot indicates for the IC (green) and SPR (blue) compressed blocking time diagram EETC driving strategies for the case Ah-Nm. The EETC driving strategy has 0.5% running time supplements for the IC and 4% running time supplements for the SPR. The dark green and dark blue blocks are the minimum buffer time of 30 s.

lower cycle time and thus may enable a possible increase in frequency. Homogenization is defined as decreasing the differences between running times on the same track section of successive trains, which can be achieved by slowing down the IC (i.e. increasing the running time supplements) or speeding up the SPR (i.e. decreasing the running time supplements). In general, homogenization has a positive effect on the infrastructure occupation.

The results of the buffer time in Table 13 show that the buffer time increases until the frequency of the number of IC-SPR train cycles can be increased for a higher service to the passengers. This effect is shown in Figure 10. For instance there is a switching point at 720 s (from 60 s to 240 s). The mesh plot of the buffer time on the left side of this figure shows the effect of the different
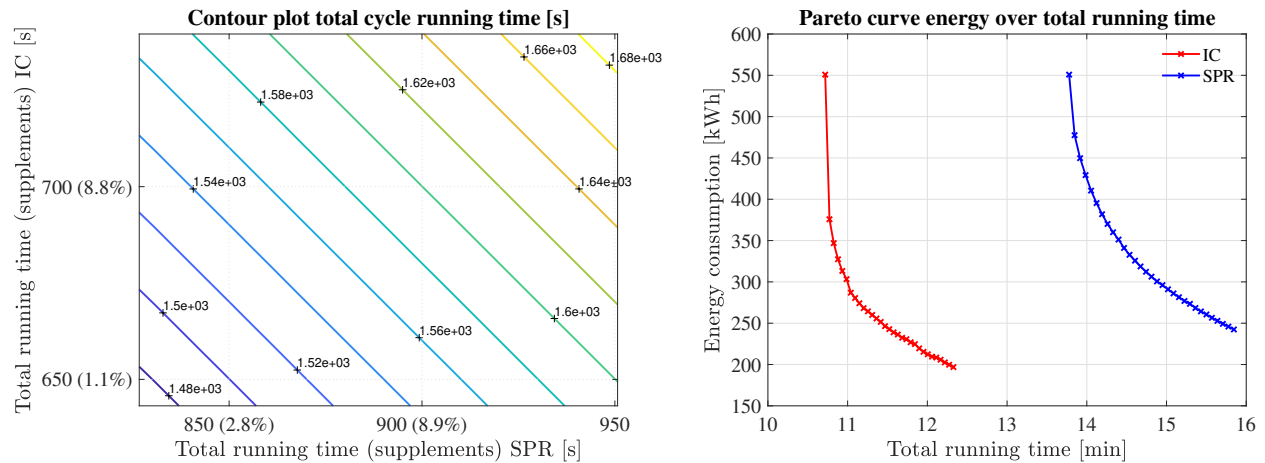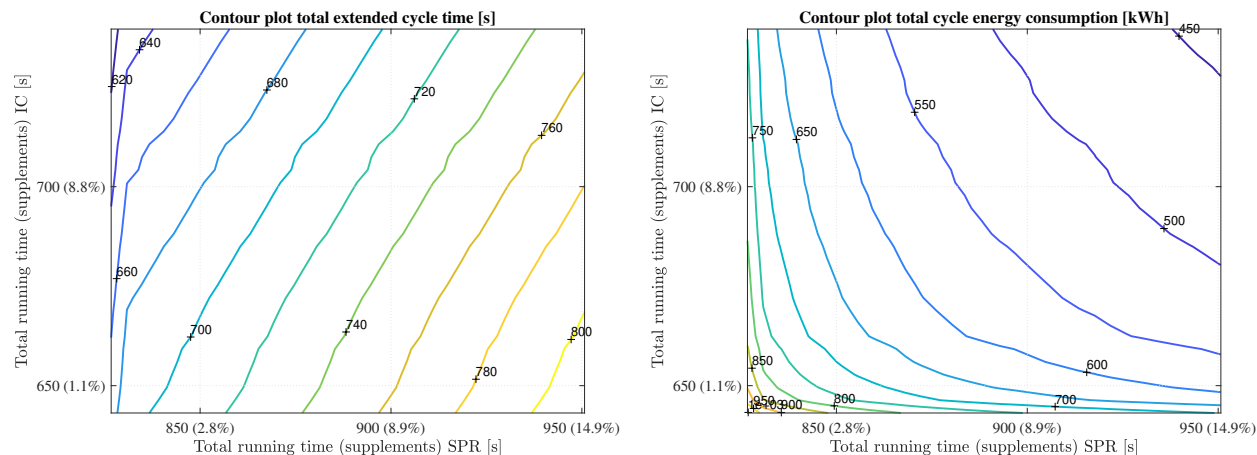
Figure 8: The left plot shows the contour plot for the case Ah-Nm for the extended cycle time over the total running time (supplements) for the SPR and IC. The right plot indicates the contour plot for the total total cycle energy consumption over the the total running time (supplements) for the SPR and IC for the case Ah-Nm.
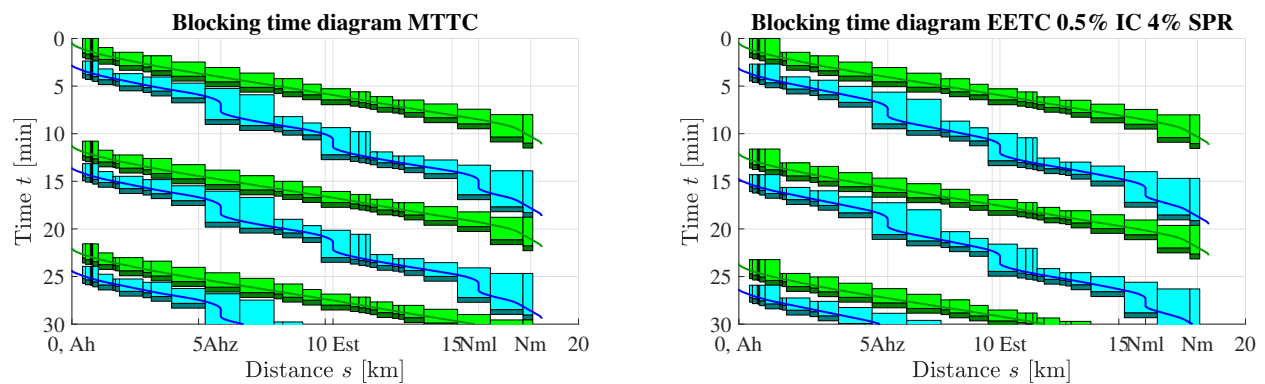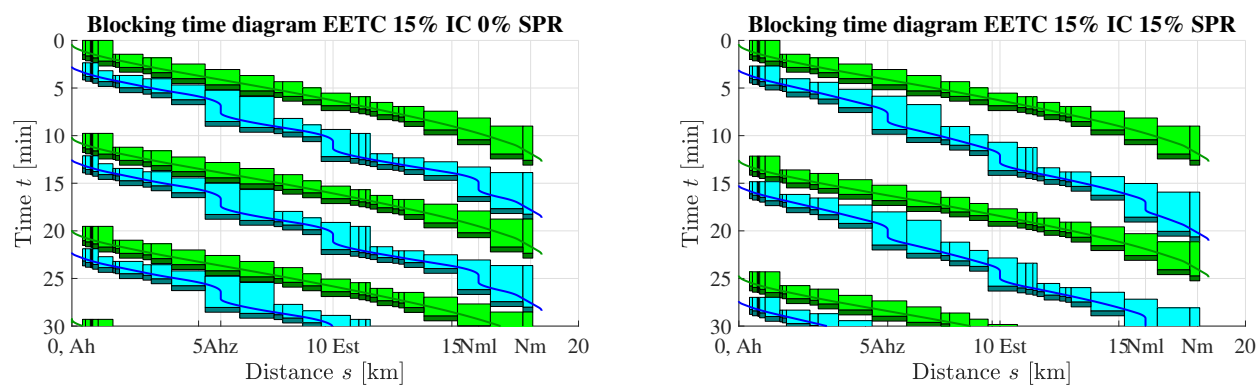

Figure 9: The left plot shows for the case Ah-Nm for the IC (green) and SPR (blue) compressed blocking time diagram for the EETC driving strategies with 15% running time supplements for the IC and 0% running time supplements for the SPR. The right plot indicates the IC (green) and SPR (blue) compressed blocking time diagram for the case Ah-Nm for the EETC driving strategies with 15% running time supplements for both the IC and SPR.

running time supplements of the SPR (x-axis) and IC (y-axis) over the buffer time (z-axis). The vertical drop in buffer time indicates the increase in frequency of both trains by one train per hour. The right plot in Figure 10 shows the effect of the extended cycle time (x-axis) over the buffer time (y-axis), which indicates a piecewise linear relationship between the two conform Eq. (16) with a jump where sufficient buffer allows an increase of the frequency. Basically, the higher the extended cycle time, the lower the buffer time. If we consider a fixed frequency of 4 IC-SPR train cycles per hour, the highest buffer time can be achieved by considering 15% running time supplements for the IC and 0% running times for the SPR, which will lead to a buffer time of 350.2 s that is determined based on extrapolation of the results in Table 13. The results of the compressed timetable are shown in the left part of Figure 9.
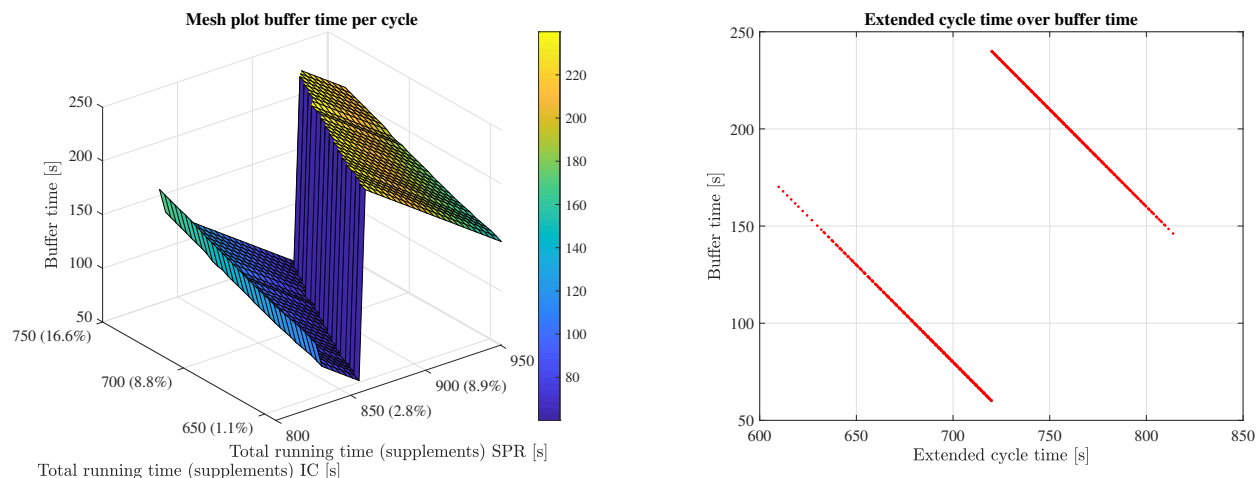
Figure 10: The left plot shows the mesh plot for the case Ah-Nm for the buffer time per cycle over the running time (supplements) of the SPR and IC. The right plot indicates the buffer time over extended cycle time for the case Ah-Nm.

The results of the energy consumption in Table 14 show that the total energy consumption decreases if the running time supplements of the IC and/or SPR increase. The highest energy savings are achieved by 15% running time supplements for both IC and SPR. The associated compressed timetable is shown in the right plot of Figure 9, indicating that the critical blocks are block 3 (after Ah for the IC-SPR order) and block 17 (at Nm for the SPR-IC order). The results are also shown in the right contour plot of Figure 8. This contour plot indicates the effect of varying the running time (supplements) of the SPR (x-axis) and varying the running time (supplements) of the IC (y-axis) on the total energy consumption. The closer the lines, the steeper the relative decrease in energy consumption compared to the extra running time. The highest relative savings are achieved with the smallest time supplement (i.e. diminishing returns) (Scheepmaker et al., 2017, 2020b). The right contour plot in Figure 8 shows that relatively higher energy savings can be achieved by including extra running time supplements for the SPR compared to the IC. For instance, the line of 700 kWh intersects the x-axis, while not intersecting the y-axis. The Pareto curve of the varying running time supplements of the IC and SPR is shown in the right plot of Figure 6. The figure clearly indicates that the steepest gradient occurs between 0% and 0.5% running time supplement, leading to the relatively largest energy savings.

4.3 Balance between objectives

In this section the balance between the different objectives of minimizing the total running time, extended cycle time and energy consumption as well as maximizing the buffer time for robustness is discussed. Optimizing each of the different objectives leads to different solutions as shown in Section 4.2. We focus both on the effect of the IC-SPR cycle as well as the effects on the IC and SPR separately. The relationship between the different single objectives is shown in the causal loop for the Intercity and Sprinter in Figure 11.

First, the causal loop in Figure 11 indicates that for the IC there is a positive relationship (reinforcing) between the objective of total running time and buffer time, i.e., an increase in the total running
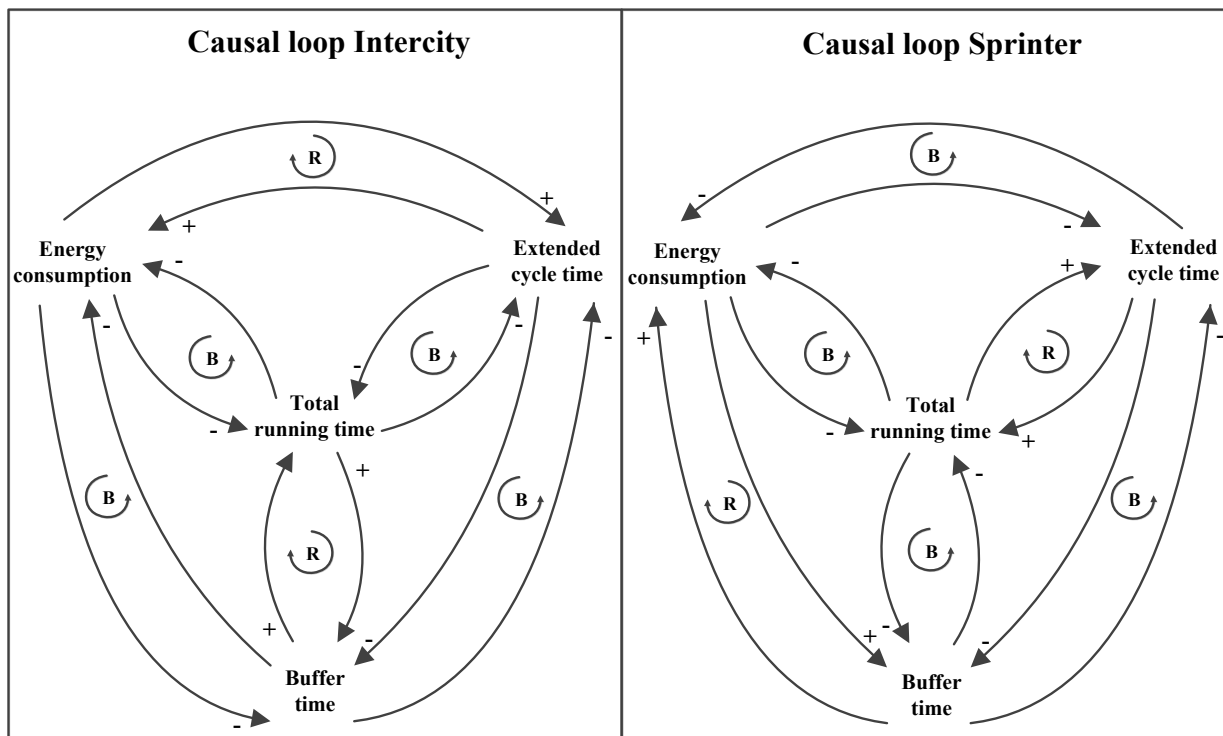
Figure 11: The left plot shows for the case Ah-Nm the causal loop diagram between the objectives for the IC. The right plot indicates for the case Ah-Nm the causal loop diagram between the objectives for the SPR (legend: R = Reinforcing, B = Balancing, + = objective at the end of the arrow is moving in the same direction as the objective at the beginning of the arrow, and − = objective at the end of the arrow is moving in the opposite direction as the objective at the beginning of the arrow).

time for the IC leads to an increase in the total buffer time for the IC-SPR cycles. For the SPR there is only a positive relationship between the total running time and extended cycle time, i.e., an increase in the total running time for the SPR leads to an increase in the extended cycle time. The relationship with all the other objectives for the IC and SPR is negative (balancing), i.e., an increase in total running time for the IC and/or SPR leads to a decrease in the other objectives. If we focus on the IC-SPR train cycle, we notice that the objective of minimizing total running time leads to the MTTC driving strategy for all trains (0% running time supplements), while considering the objectives of maximizing robustness, minimizing capacity or energy consumption leads to a certain optimal amount of running time supplements. The most clear trade-off is between minimizing the total running time and minimizing the energy consumption, because for energy minimization the trains should have the maximum possible amount of running time supplements. However, as explained in Section 4.2 the relative energy savings achieved by extra running time supplements decreases for higher supplements (diminishing returns).

Second, we see that there is a clear relationship between infrastructure occupation and robustness. As stated in Section 2.4 by Eq. (16) and also shown in the right plot in Figure 10 there is a negative linear relationship between the extended cycle time and buffer time. This can also be observed from the causal loop in Figure 11 (balancing between the extended cycle time and buffer time for

both the IC and SPR). If we consider a fixed frequency of IC-SPR train cycles per hour, we see that higher extended cycle times lead to lower buffer time.

Third, there is a reinforcing relationship between the extended cycle time and energy consumption for the IC and a balancing relationship between the extended cycle time and energy consumption for the SPR, see Figure 11. This can also be seen in Figure 12. Each of the lines in the left plot in the figure represents the fixed percentage of running time supplements of the IC, while the running time supplements of the SPR are varied. The right plot in the figure indicates the opposite by fixing the running time supplements of the SPR and varying the running time supplements of the IC. The figures clearly indicate that higher amount of supplements for the SPR leads to a higher extended cycle time, while higher amounts of supplements for the IC leads to a lower extended cycle time (homogenization). Moreover, Figure 12 shows the effect of diminish returns of the extra running time compared to the extra extended cycle time by the gradient of the curve.
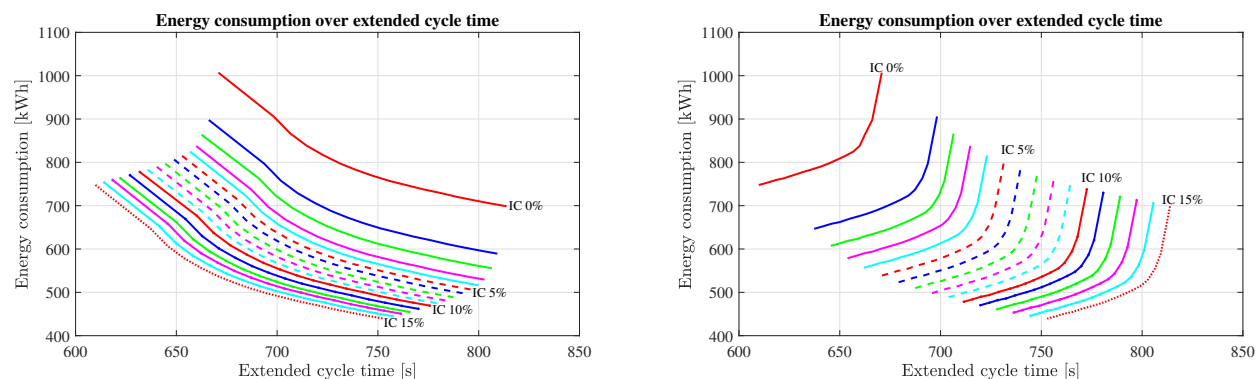
Figure 12: The left plot shows the energy consumption over the extended cycle time for the case Ah-Nm for fixed running time supplements of the IC and varying running time supplements for the SPR. The right plot indicates the energy consumption over the extended cycle time for fixed running time supplements of the SPR and varying running time supplements for the IC for the case Ah-Nm.

Fourth, the relationship between buffer time and energy consumption is balancing for the IC and reinforcing for the SPR, see Figure 11. Robustness can be improved by increasing the buffer time, which is achieved by adding large amount of running time supplements to the IC and none to the SPR (MTTC). This means that the fastest train gains the highest running time supplements. However, for the objective of minimizing the energy consumption relatively more energy savings can be achieved by adding extra running time supplement to the slowest train (SPR), while overall the most energy can be saved by giving all trains the maximum amount of running time supplements.

4.4 Multiple objectives

In this section we consider the optimal solution of the multiple objectives as described in Section 4.2. We use two different methods to compute the optimal solutions. The first method is based on the weighted sum and the second method is based on the standard Euclidean distance. We start in Section 4.4.1 with a sensitivity analysis for determining the scaling and weight factors that are needed for the weighed sum method. Section 4.4.2 discusses the results of the optimization with the three objectives of minimizing total travel time, extended cycle time and maximizing the buffer

time. The effects of including energy minimization to the other three objectives is discussed in Section 4.4.3.

Sensitivity analysis scaling and weight factors

In this section we discuss the sensitivity analysis to determine the scaling and weight factors for the weighted sum method. We first give the outline of the approach in five steps. Afterwards, we present the main results of the sensitivity analysis. The results are used to compute the different multiple objective values using the two methods.

We started by doing a sensitivity analysis to determine the scaling factors of the three-objective optimization function, i.e., the total running time, extended cycle time, and total buffer time. We considered the minimum, medium and maximum relationship instead of the average relationship as given by Eq. (18). Second, we did a sensitivity analysis for the weight factors of the three objectives, where we assumed $w_4 = 0$. We started by finding the correlation between the total running time and extended cycle time by varying the weight factor w_1 (and w_2) on the interval $[0, 0.66]$, with a constant weight factor for the buffer time (i.e. $w_3 = 0.33$). Afterwards, we looked for the correlation between the extended cycle time and total buffer time by varying the weight factor w_2 (and w_3) on the interval $[0, 0.66]$ given a constant value of the weight factor for the total running time (i.e. $w_1 = 0.33$). Third, we determined the scaling factor for energy consumption ω by including the energy consumption objective with the three other objectives and varying the scaling factor. We varied the scaling factor ω on the interval $[0, 20]$ while using equal weight factors for all objectives in order to scale the energy consumption objective (i.e. $w_1 = w_2 = w_3 = w_4 = 0.25$). Fourth, given the relationship between the three objectives and the scaling factor for the energy consumption we applied the sensitivity analysis of the weight factor w_4 on the interval $[0, 1]$ for the energy consumption considering the four-objective optimization problem. We varied the value of w_4 and we assumed the other weight factors to be equal to each other (i.e. $w_1 = w_2 = w_3$). Fifth, we investigated the relationship between the extended cycle time that is related to the infrastructure occupation, and the total energy consumption by doing two sensitivity analyse. During the first sensitivity analysis we varied the weight factors w_2 and w_4 between 0 and 0.5 and we set the other weight factors equal to 0.25 (i.e. $w_1 = w_3 = 0.25$). We added a second sensitivity scenario in which we considered only the objectives of extended cycle time and energy consumption by setting $w_1 = w_3 = 0$, and we varied the values of w_2 and w_4 between 0 and 1.

The results of the scaling factors given in Eq. (18) show that the scaling factors are robust. The sensitivity analysis of the weight factors of the three different objectives indicate that three objectives are stable for varying the different single weight factors. Since the three objectives are already scaled by Eq. (18), we choose equal weights for them, i.e. $w_1 = w_2 = w_3 = 0.33$. The results of the sensitivity analysis of the scaling factor ω for the energy consumption are shown in Figure 13. The left plot in this figure indicates the effect of varying the scaling factor of the energy consumption ω for the single objectives (left y-axis) and for the multiple objectives (right y-axis), due to the different magnitude. The right plot shows the optimal solution for the relative amount of running time supplements for the IC and SPR that leads to the optimal value given the scaling factor value ω. The results indicate that Z_E is not sensitive on different intervals of ω. Stability for the objectives is reached when $\omega \in [4.6, 13]$, however, this leads to relatively large amount of running time supplements (15% IC and 11.5% SPR). From a practical perspective the running time

EJTIR 21(4), 2021, pp.1-42
Scheepmaker and Goverde
Multi-objective railway timetabling including energy-efficient train trajectory optimization

26
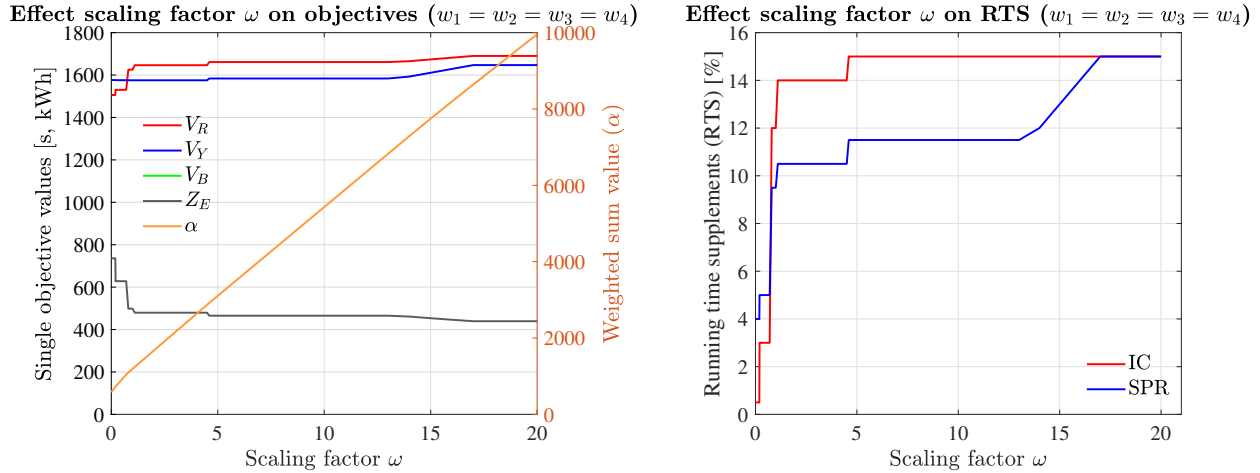
Figure 13: The left plot shows the sensitivity analysis by varying the scaling factor of the energy consumption ω related to the single objectives (left y-axis) and weighted sum value (right y-axis). The right plot indicates the running time supplements (RTS) for the IC and SPR given the varying weight factor of the energy consumption ω.

supplements at NS should be at least 8% and not too big, therefore, we choose the 12% for the IC and 9.5% for the SPR which leads to a scaling factor $\omega = 1$. We choose equal weight factors for all objectives in the rest of the paper based on the sensitivity analysis of weight factor w_4, i.e. $w_1 = w_2 = w_3 = w_4 = 0.25$, because V_R, V_c, V_B and V_E are not sensitive on different intervals of w_4. The results of the first sensitivity analysis between the extended cycle time and energy consumption indicate that both V_c and V_B are relatively stable for the varying weight factor for the energy consumption, and the capacity consumption is about 80%. The results of the second sensitivity analysis indicate that the lower the value of w_4, the higher the total energy consumption and the lower the extended cycle time, and thus the lower the infrastructure occupation when the frequency remains the same (i.e. 4 IC-SPR cycles per hour). In addition, low values of w_4 lead to a low amount of running time supplements for the SPR (i.e. homogenization), while high values of w_4 lead to a high amount of running time supplement for the SPR. The relative amount of running time supplements for the IC remains constant for varying values of w_4 (15% running time supplements).

Results for multiple objectives without energy consumption

We start by analyzing the results considering the multiple-objective function with the three objectives: total running time, extended cycle time and total buffer time (thus without energy consumption). The top 10 Pareto-optimal solutions can be found in Table 2. The top 10 of optimal values are sorted according to the order of the weighted sum (from low to high), because in this method the different objectives are scaled and weighted. The optimal solution ($\alpha = 193.7$) is achieved by 0.5% running time supplements for the IC and 4% running time supplements for the SPR. This leads to relatively low amount of total running time (1506 s) for the IC-SPR cycle as well as high amount of buffer time (239 s, close to the maximum buffer time in Table 13). The total energy consumption is about 736 kWh and the capacity consumption is about 80%. The drawback for this

solution is that the extended cycle time is relatively high, which leads to a maximum frequency of 4 IC-SPR cycles per hour. In addition, the optimal solution considering the weighed sum method is the same as considering the Euclidian distance, although their value is different ($\alpha = 193.7$ and $\beta = 0.5674$). This is caused by the fact that the total running time is close to its minimum value and the buffer time is almost its maximum value. The right plot in Figure 7 shows the resulting compressed timetable for the optimal solution with the critical block sections 3 (IC-SPR) and 17 (SPR-IC). The top 10 of α-optimal solutions shows that optimal solutions consider very low amount of running time supplements for the IC and slightly higher amount of running time supplements for the SPR. In addition, the top-10 order of the α-optimal solutions are different compared to the β-optimal solutions, due to the scaling of the objectives in the weighted sum method.

In the Netherlands the norm for running time supplements for each train is at least 8% for timetable stability. If we include this NS constraint to determine the optimal solution according to the weighted sum method, the running time supplements should be 10.5% for the IC and 8.5% for the SPR ($\alpha = 225.6$) as can be seen in Table 2. The result is far away from the optimal solution without the constraint of at least 8% running time supplements for the IC and SPR, which leads to relatively a high amount of running time. The compressed timetable of this scenario is shown in the left plot in Figure 14, indicating the critical block sections 3 (IC-SPR) and 17 (SPR-IC). The main difference compared to the top 10 α-optimal solutions is the increase in total running time. Therefore, this optimal solution could only be achieved by adding the constraints of at least 8% running time supplements given the three-objective optimization.
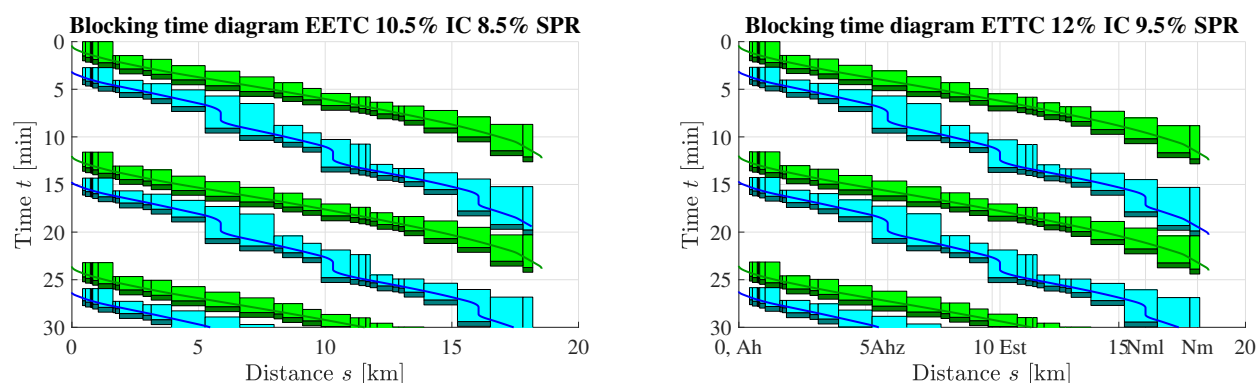
Figure 14: The left plot shows for the case Ah-Nm for the IC (green) and SPR (blue) compressed blocking time diagram for the EETC driving strategies with 10.5% running time supplements for the IC and 8.5% running time supplements for the SPR. The right plot indicates the IC (green) and SPR (blue) compressed blocking time diagram for the case Ah-Nm for the EETC driving strategies with 12% running time supplements for the IC and 9.5% running time supplements for the SPR.

Results for all objectives including energy consumption

Here we consider the four objectives in the multiple-objective optimization: total running time, extended cycle time, buffer time, and energy consumption. The results can be found in Table 3. The optimal solution according to the weighted sum method ($\alpha = 298.3$) is achieved by 12% running time supplements for the IC and 9.5% running time supplements for the SPR. This solution complies to

Table 2: First 10 Pareto-optimal solutions and NS constrained optimal solution (No. α 21) with 30 s minimum buffer time considering the objectives total running time Z_R, extended cycle time Z_c and buffer time Z_b for the real-world case Ah-Nm using the weighted sum method (sorted from low to high according to α).

No. α	No. β	RTS IC (%)	RTS SPR (%)	Z_R (s)	Z_c (s)	Z_b (s)	Z_E (kWh)	f (-)	C (%)	α	β
1	1	0.5	4.0	1506.0	720.6	239.4	735.8	4	80.1	193.7	0.5674
2	11	1.5	4.5	1516.6	721.2	238.8	678.6	4	80.1	199.7	0.5858
3	20	3.0	5.0	1530.4	720.3	239.7	628.0	4	80.0	200.5	0.6073
4	2	0.0	4.5	1502.8	723.0	237.0	816.3	4	80.3	202.6	0.5748
5	13	1.0	4.5	1513.3	722.6	237.4	698.1	4	80.3	204.2	0.5869
6	32	4.0	5.5	1540.9	721.4	238.6	606.9	4	80.2	208.6	0.6350
7	22	2.5	5.0	1527.2	722.8	237.2	644.4	4	80.3	209.7	0.6118
8	14	0.5	4.0	1510.1	724.8	235.2	727.0	4	80.5	212.5	0.5929
9	42	5.0	6.0	1551.5	721.6	238.4	590.0	4	80.2	213.0	0.6616
10	21	2.0	5.0	1523.9	724.0	236.0	654.3	4	80.4	213.7	0.6114
21	204	10.5	8.5	1607.5	720.2	239.8	520.8	4	80.0	225.6	0.8265

Legend: α = weighted sum, β = standardized Euclidean distance, IC = Intercity, SPR = Sprinter, RTS = running time supplements, Z_R = minimum running time objective, Z_c = minimum extended cycle time objective, Z_b = maximum buffer time objective, Z_E = minimum energy consumption objective, f = frequency of IC-SPR cycles per hour, C = capacity consumption.

the NS constraint optimal solution of at least 8% running time supplements for the IC and the SPR. The compressed timetable of this scenario can be seen in the right plot in Figure 14, indicating that the critical block sections are block section 3 (IC-SPR) and 17 (SPR-IC). The optimal solution leads to a total running time of 1625 s, an extended cycle time of 720 s (frequency of 4 IC-SPR cycles per hour), 240 s buffer time, a capacity consumption of 80%, and an energy consumption of 498 kWh. We can see that including the energy consumption into the multiple-objective optimization leads to higher running times, but the resulting extended cycle time and buffer time are almost the same. Therefore, including energy consumption in the multiple-objective optimization only influences the total running time (i.e. balance total running time and energy consumption). Analyzing the top 10 optimal solutions according to the weighted sum method shows that the running time supplements of the IC vary between 7% and 14.5% while the running time supplements of the SPR vary between 7.5% and 11% and are in general relatively smaller than the IC. The optimal values of the extended cycle time and buffer time remain about the same (small fluctuations), while there are bigger fluctuations in the total running time and energy consumption. Moreover, the results of the top 10 α-optimal solutions are completely different compared to the β-optimal solutions, because in the weighted sum method all different objectives are scaled to each other, and in the standardized Euclidean distance the variables are only normalized on the interval [0, 1].

4.5 Effect of varying minimum buffer time

We investigated the effect of varying the minimum buffer time on the optimal solution. Therefore, we included two scenarios: one with 0 s (Table 4) and one with 60 s (Table 5) minimum buffer time for each train instead of 30 s (Table 3). Since the minimum buffer time is constant for all trains over the complete trajectory, the results indicate that the optimal solutions considering the

Table 3: First 10 Pareto-optimal solutions with 30 s minimum buffer time considering the objectives total running time Z_R, extended cycle time Z_c, buffer time Z_b and energy consumption Z_E for the real-world case Ah-Nm using the weighted sum method (sorted from low to high according to α).

No. α	No. β	RTS IC (%)	RTS SPR (%)	Z_R (s)	Z_c (s)	Z_b (s)	Z_E (kWh)	f (-)	C (%)	α	β
1	205	12.0	9.5	1625.4	720.2	239.8	498.4	4	80.0	298.3	0.8955
2	271	13.0	10.0	1636.0	720.1	239.9	489.9	4	80.0	298.4	0.9319
3	344	14.0	10.5	1646.5	720.1	239.9	479.4	4	80.0	298.5	0.9694
4	116	10.5	8.5	1607.5	720.2	239.8	520.8	4	80.5	299.4	0.8389
5	152	13.0	9.0	1614.9	720.6	239.4	510.6	4	80.1	299.9	0.8624
6	44	8.0	7.5	1583.2	721.5	238.5	545.2	4	80.2	303.7	0.7741
7	68	9.0	8.0	1593.7	721.8	238.2	532.9	4	80.2	303.9	0.8028
8	25	7.0	7.0	1572.6	721.4	238.6	558.6	4	80.2	303.9	0.7489
9	197	11.5	9.5	1622.2	722.1	237.9	501.4	4	80.2	304.3	0.8905
10	414	14.5	11.0	1653.9	722.0	238.0	473.1	4	80.2	304.9	1.0020

Legend: α = weighted sum, β = standardized Euclidean distance, IC = Intercity, SPR = Sprinter, RTS = running time supplements, Z_R = minimum running time objective, Z_c = minimum extended cycle time objective, Z_b = maximum buffer time objective, Z_E = minimum energy consumption objective, f = frequency of IC-SPR cycles per hour, C = capacity consumption.

weighted sum and the Euclidean distance remain the same, except the value of the weighted sum. The change in buffer time only leads to a different total buffer time, extended cycle time, frequency and capacity consumption. In general higher minimum buffer time leads to lower frequencies of IC-SPR cycles per hour. If we consider a fixed frequency of IC-SPR cycles per hour, then the higher the minimum buffer time, the higher the capacity consumption. We can thus conclude that the change in minimum buffer time does not influence the results for the weighted sum and the standard Euclidean distance.

4.6 Discussion of the main results

In this section we discuss the main results achieved by the case study. We make a distinction between results of the single objectives, the interaction between objectives, the sensitivity analysis for the scaling and weight factors, and the multiple objectives. The main results of the case study are the causal loop diagram in Figure 11 that indicates the relationship between the objectives, and the application of two methods to compute the optimal solutions, which show that only the total running time is influenced by including the energy consumption in the multiple-objective optimization.

First, we focus on the main results for the single objectives. Basically, optimizing for the different single objectives leads to different results. The MTTC driving strategy gives the optimal timetable considering the total running times. Homogenization by increasing the running times of the SPR and decreasing the running times of the IC leads to the optimal solution for minimizing the extended cycle time, which also results into the highest buffer times (if the frequency remains the same). Minimizing the total traction energy consumption leads to maximum amount of running time supplements for the EETC driving strategy of both IC and SPR.

Table 4: First 10 Pareto-optimal solutions with 0 s minimum buffer time considering the objectives total running time Z_R, extended cycle time Z_c, buffer time Z_b and energy consumption Z_E for the real-world case Ah-Nm using the weighted sum method (sorted from low to high according to α).

No. α	No. β	RTS IC (%)	RTS SPR (%)	Z_R (s)	Z_c (s)	Z_b (s)	Z_E (kWh)	f (-)	C (%)	α	β
1	205	12.0	9.5	1625.4	720.2	179.8	498.4	5	91.7	455.0	0.8955
2	271	13.0	10.0	1636.0	720.1	179.9	489.9	5	91.7	455.2	0.9319
3	344	14.0	10.5	1646.5	720.1	179.9	479.4	5	91.7	455.3	0.9694
4	116	10.5	8.5	1607.5	720.2	179.8	520.8	5	91.7	456.2	0.8389
5	152	13.0	9.0	1614.9	720.6	179.4	510.6	5	91.7	456.7	0.8624
6	44	8.0	7.5	1583.2	721.5	178.5	545.2	5	91.9	460.4	0.7741
7	68	9.0	8.0	1593.7	721.8	178.2	532.9	5	91.9	460.7	0.8028
8	25	7.0	7.0	1572.6	721.4	178.6	558.6	5	91.9	460.7	0.7489
9	197	11.5	9.5	1622.2	722.1	177.9	501.4	5	92.0	461.0	0.8905
10	414	14.5	11.0	1653.9	722.0	178.0	473.1	5	92.0	461.7	1.0020

Legend: α = weighted sum, β = standardized Euclidean distance, IC = Intercity, SPR = Sprinter, RTS = running time supplements, Z_R = minimum running time objective, Z_c = minimum extended cycle time objective, Z_b = maximum buffer time objective, Z_E = minimum energy consumption objective, f = frequency of IC-SPR cycles per hour, C = capacity consumption.

Table 5: First 10 Pareto-optimal solutions with 60 s minimum buffer time considering the objectives total running time Z_R, extended cycle time Z_c, buffer time Z_b and energy consumption Z_E for the real-world case Ah-Nm using the weighted sum method (sorted from low to high according to α).

No. α	No. β	RTS IC (%)	RTS SPR (%)	Z_R (s)	Z_c (s)	Z_b (s)	Z_E (kWh)	f (-)	C (%)	α	β
1	205	12.0	9.5	1625.4	720.2	299.8	498.4	4	86.7	141.5	0.8955
2	271	13.0	10.0	1636.0	720.1	299.9	489.9	4	86.7	141.6	0.9319
3	344	14.0	10.5	1646.5	720.1	299.9	479.4	4	86.7	141.7	0.9694
4	116	10.5	8.5	1607.5	720.2	299.8	520.8	4	86.7	142.6	0.8389
5	152	13.0	9.0	1614.9	720.6	299.4	510.6	4	86.7	143.1	0.8624
6	44	8.0	7.5	1583.2	721.5	298.5	545.2	4	86.8	146.9	0.7741
7	68	9.0	8.0	1593.7	721.8	298.2	532.9	4	86.9	147.2	0.8028
8	25	7.0	7.0	1572.6	721.4	298.6	558.6	4	86.8	147.2	0.7489
9	197	11.5	9.5	1622.2	722.1	297.9	501.4	4	86.9	147.5	0.8905
10	414	14.5	11.0	1653.9	722.0	298.0	473.1	4	86.9	148.2	1.0020

Legend: α = weighted sum, β = standardized Euclidean distance, IC = Intercity, SPR = Sprinter, RTS = running time supplements, Z_R = minimum running time objective, Z_c = minimum extended cycle time objective, Z_b = maximum buffer time objective, Z_E = minimum energy consumption objective, f = frequency of IC-SPR cycles per hour, C = capacity consumption.

Second, the main results regarding the interaction between the different single objectives indicates the clear linear balancing relationship between the extended cycle time and the buffer time. There is also a balancing relationship between the objectives of total running time and energy consumption. The interaction with the other objectives depends for the IC or SPR whether it is balancing or reinforcing.

Third, in order to apply the weighted sum method, we defined the scaling and weight factors. The result indicate that the average ratio between the extended cycle time and total running time, and between the total buffer time and total running time can be used as scaling factor, where the the total running time is the reference (scaling factor 1). In addition, the sensitivity analysis indicates that the scaling factor 1 for the total energy consumption leads to the best balanced optimal results given the practical constraint of at least 8% running time supplements for each train. We also applied a sensitivity analysis for the weight factors and found that equal weight factors for all objectives leads to the best balanced results, because the objective values were already scaled. Finally, we did a sensitivity analysis for the weight factors of extended cycle time and energy consumption, which indicates that the extended cycle time varies limited. Only by excluding the objectives of total running time and total buffer time, we found that the extended cycle time (and thus the infrastructure occupation) varies for different weight factors and that there is a balancing relationship between the extended cycle time and total energy consumption.

Fourth, the main results regarding the multiple objectives show that only the objective of total running time is influenced by including the objective of total energy consumption in the multiple-objective optimization (i.e. the extended cycle time and buffer time remain the same). The results also indicates that (considering the three objectives of total running time, extended cycle time and buffer time) there is only a trade-off between the extended cycle time (and thus frequency) and the buffer time (i.e. the total running time remain the same). In addition, the results show that changing the minimum buffer time does not influence the optimal results (only changes the extended cycle time and total buffer time). Finally, the results of the weighted sum and standard Euclidean distance method are different when all four objectives are considered. This is caused by the the fact that the weighted sum method includes scaling of the different single objectives, which is not considered for the standard Euclidean distance method.

5. Conclusions

We considered the topic of energy-efficient train timetabling by investigating the multiple-objective optimization problem for a cyclic pattern of trains on a railway line. The aim was to minimize the total running time, the infrastructure occupation (by the extended cycle time) and energy consumption and to maximize the robustness (by the total buffer time) of the timetable, while guaranteeing a conflict-free timetable using the blocking time theory. We introduced the term extended cycle time that expanded the cycle time with a fixed minimum buffer time that is commonly applied by railway undertakings and infrastructure managers to cope with robustness. We investigated the effect of including energy consumption to the multiple-objective timetable optimization problem of total running time, infrastructure occupation and robustness.

We used a constructive brute force search algorithm in order to determine the optimal objective values. We first computed the different driving strategies including the blocking times by varying

the running time supplements for all trains. Then we applied the timetable compression method to compute the minimum extended cycle time and the buffer time between each train cycle. Thus, we computed the single objective values for the total running time, extended cycle time, buffer time and energy consumption, using the given amount of running times of the trains. Finally, we used two different methods to compute the multiple-objective solution: the weighted sum and the standard Euclidean distance method. The methods used in this paper basically transform the multiple-objective optimization functions into a single objective function. Future research will focus on different methods to solve the multiple-objective optimization problem directly by determining the Pareto frontier instead of a single Pareto optimal solution, such as the ε-constraint method (Yan et al., 2019).

We applied the methods to a real-world case study on the Dutch railway corridor with alternating Intercity and Sprinter train services without intermediate overtaking. There is a clear linear balancing relationship between the extended cycle time and buffer time, which indicates that an increase in the extended cycle time leads to a decrease in the buffer time. In addition, we found a balancing relationship between the total running time and energy consumption without influencing the infrastructure occupation and robustness. We also observed a balancing relationship between the extended cycle time and total energy consumption. Finally, we found that changing the minimum buffer time does not influence the optimal solution.

We conclude that taking energy consumption into account is a good method for RUs to balance total running time without affecting capacity and robustness. RUs should note that minimizing the infrastructure occupation results into homogenization, which leads to limited running time supplements for the slowest train, while high amount of running time supplements are allocated to the fastest train. Minimizing the cycle times enables RUs to increase the frequency of trains, but this reduces the total buffer time.

In this paper we focused on changing the extended cycle time by influencing the running times. The extended cycle time can also be improved by including overtaking possibilities for the IC, skipping stops for the SPR or changing the rolling stock formation. Future research will focus on the effect of these measures on the results of the multiple-objective optimization.

Regenerative braking can lead to extra energy savings and can reduce the power peak supply around stations, but can also influence the trade-off with the other three objectives. Therefore, future research will focus on synchronizing accelerating and regenerative braking trains by including the transmission of regenerated energy over the power supply system in the multiple-objective optimization problem.

Finally, we applied an integrated approach for the multiple-objective timetable optimization problem. However, this approach increases the complexity of the model. In addition, the results also indicated relationships between mainly two objectives (with limited effect on the other objectives). Therefore, similar to Goverde et al. (2016), future research could focus on a sequential approach to solve the problem, without substantial loss of optimality. However, instead of considering the energy consumption after the other objectives, the sequential approach could start by first optimizing both the objectives of total running time and energy consumption. Afterwards, the infrastructure occupation and robustness can be optimized, given constraints regarding the total running time and energy consumption.

EJTIR 21(4), 2021, pp.1-42
Scheepmaker and Goverde
Multi-objective railway timetabling including energy-efficient train trajectory optimization

33

Acknowledgements

References

Albrecht, A. R., Howlett, P. G., and Pudney, P. J. (2020). Optimal driving strategies for two successive trains on level track with safe separation. *IEEE Transactions on Intelligent Transportation Systems*, pages 1–16.

Albrecht, T. (2004). Reducing power peaks and energy consumption in rail transit systems by simultaneous train running time control. In Allen, J., Brebbia, A., Hill, R. J., Sciutto, G., and Sone, S., editors, *Computers in Railways IX*, pages 885–894. WIT Press, Southampton, UK.

Arboleya, P., Mayet, C., Mohamed, B., Aguado, J. A., and De la Torre, S. (2020). A review of railway feeding infrastructures: Mathematical models for planning and operation. *eTransportation*, 5:100063.

Betts, J. T. (2010). *Practical Methods for Optimal Control and Estimation Using Nonlinear Programming*. Advances in Design and Control. SIAM, Philadelphia, PA, USA.

Bešinović, N. and Goverde, R. M. P. (2018). Capacity assessment in railway networks. In Borndörfer, R., Klug, T., Lamorgese, L., Mannino, C., Reuther, M., and Schlechte, T., editors, *Handbook of Optimization in the Railway Industry*, pages 25–45. Springer International Publishing, Cham, Switzerland.

Bešinović, N., Goverde, R. M. P., and Quaglietta, E. (2017). Microscopic models and network transformations for automated railway traffic planning. *Computer-Aided Civil and Infrastructure Engineering*, 32(2):89–106.

Bešinović, N., Goverde, R. M. P., Quaglietta, E., and Roberti, R. (2016). An integrated micro–macro approach to robust railway timetabling. *Transportation Research Part B: Methodological*, 87:14–32.

Binder, A. and Albrecht, T. (2013). Timetable evaluation and optimization under consideration of the stochastical influence of the dwell times. In *Proceedings of the 3rd International Conference on Models and Technologies for Intelligent Transportation Systems 2013*, pages 471–481.

Brünger, O. and Dahlhaus, E. (2014). Running time estimation. In Hansen, I. A. and Pachl, J., editors, *Railway Timetabling & Operations*, pages 65–89. Eurailpress, Hamburg, Germany.

Cacchiani, V., Galli, L., and Toth, P. (2015). A tutorial on non-periodic train timetabling and platforming problems. *EURO Journal on Transportation and Logistics*, 4(3):285–320.

Cacchiani, V., Huisman, D., Kidd, M., Kroon, L. G., Toth, P., Veelenturf, L. P., and Wagenaar, J. C. (2014). An overview of recovery models and algorithms for real-time railway rescheduling. *Transportation Research Part B: Methodological*, 63:15–37.

Cacchiani, V. and Toth, P. (2012). Nominal and robust train timetabling problems. *European Journal of Operational Research*, 219(3):727–737.

Caprara, A., Kroon, L. G., Monaci, M., Peeters, M., and Toth, P. (2007). *Chapter 3 Passenger Railway Optimization*, volume 14, pages 129–187. Elsevier.

Cucala, A. P., Fernández, A., Sicre, C., and Domínguez, M. (2012). Fuzzy optimal schedule of high speed train operation to minimize energy consumption with uncertain delays and driver's behavioral response. *Engineering Applications of Artificial Intelligence*, 25(8):1548–1557.

Davis, W. (1926). The tractive resistance of electric locomotives and cars. *General Electric Review*, 29.

Ding, Y., Liu, H., Bai, Y., and Zhou, F. (2011). A Two-level Optimization Model and Algorithm for Energy-Efficient Urban Train Operation. *Journal of Transportation Systems Engineering and Information Technology*, 11(1):96–101.

Garg, D., Patterson, M. A., Hager, W. W., Rao, A. V., Benson, D. A., and Huntington, G. T. (2009). An overview of three pseudospectral methods for the numerical solution of optimal control problems. *Advances in the Astronautical Sciences*, 135(1):475–487.

Goverde, R. M. P., Bešinović, N., Binder, A., Cacchiani, V., Quaglietta, E., Roberti, R., and Toth, P. (2016). A three-level framework for performance-based railway timetabling. *Transportation Research Part C: Emerging Technologies*, 67:62–83.

Goverde, R. M. P., Corman, F., and D'Ariano, A. (2013). Railway line capacity consumption of different railway signalling systems under scheduled and disturbed conditions. *Journal of Rail Transport Planning & Management*, 3(3):78–94.

Goverde, R. M. P. and Hansen, I. A. (2013). Performance indicators for railway timetables. In *2013 IEEE International Conference on Intelligent Rail Transportation Proceedings*, pages 301–306.

Goverde, R. M. P., Scheepmaker, G. M., and Wang, P. (2021). Pseudospectral optimal train control. *European Journal of Operational Research*, 292(1):353–375.

Howlett, P. G. (2016). A new look at the rate of change of energy consumption with respect to journey time on an optimal train journey. *Transportation Research Part B: Methodological*, 94:387–408.

Howlett, P. G. and Pudney, P. J. (1995). *Energy-Efficient Train Control*. Springer, London, UK.

Jensen, L. W., Landex, A., Nielsen, O. A., Kroon, L. G., and Schmidt, M. (2017). Strategic assessment of capacity consumption in railway networks: Framework and model. *Transportation Research Part C: Emerging Technologies*, 74:126–149.

Kroon, L. G., Huisman, D., and Maróti, G. (2014). Optimisation models for railway timetabling. In Hansen, I. A. and Pachl, J., editors, *Railway Timetabling & Operations*, book section 8, pages 155–173. Eurailpress, Hamburg, Germany.

Li, X. and Lo, H. K. (2014a). An energy-efficient scheduling and speed control approach for metro rail operations. *Transportation Research Part B: Methodological*, 64:73–89.

Li, X. and Lo, H. K. (2014b). Energy minimization in dynamic train scheduling and control for metro rail operations. *Transportation Research Part B: Methodological*, 70:269–284.

Luan, X., Wang, Y., De Schutter, B., Meng, L., Lodewijks, G., and Corman, F. (2018a). Integration of real-time traffic management and train control for rail networks - part 1: Optimization problems and solution approaches. *Transportation Research Part B: Methodological*, 115:41–71.

Luan, X., Wang, Y., De Schutter, B., Meng, L., Lodewijks, G., and Corman, F. (2018b). Integration of real-time traffic management and train control for rail networks - part 2: Extensions towards energy-efficient train operations. *Transportation Research Part B: Methodological*, 115:72–94.

Lusby, R. M., Larsen, J., and Bull, S. (2018). A survey on robustness in railway planning. *European Journal of Operational Research*, 266(1):1–15.

Lusby, R. M., Larsen, J., Ehrgott, M., and Ryan, D. (2011). Railway track allocation: models and methods. *OR Spectrum*, 33(4):843–883.

Marler, R. T. and Arora, J. S. (2004). Survey of multi-objective optimization methods for engineering. *Structural and Multidisciplinary Optimization*, 26(6):369–395.

NS (2020). *TreinPlein*. https://treinplein.net.

Pachl, J. (2009). *Railway Operation and Control*. VTD Rail Publishing, Mountlake Terrace, WA, USA.

Pachl, J. (2014). Timetable design principles. In Hansen, I. A. and Pachl, J., editors, *Railway Timetabling & Operations*, pages 13–46. Eurailpress, Hamburg, Germany.

Panou, K., Tzieropoulos, P., and Emery, D. (2013). Railway driver advice systems: Evaluation of methods, tools and systems. *Journal of Rail Transport Planning and Management*, 3(4):150–162.

Peña-Alcaraz, M., Fernandéz, A., Cucala, A., Ramos, A., and Pecharromán, R. R. (2012). Optimal underground timetable design based on power flow for maximizing the use of regenerative-braking energy. *Proceedings of the Institution of Mechanical Engineers, Part F: Journal of Rail and Rapid Transit*, 226(4):397–408.

ProRail (2020). *RailDocs*. https://www.raildocs.nl/raildocs/tekeningen.

Radtke, A. (2014). Infrastructure modelling. In Hansen, I. A. and Pachl, J., editors, *Railway Timetabling & Operations*, pages 47–63. Eurailpress, Hamburg, Germany.

Rao, A. V., Benson, D., Darby, C., Mahon, B., Francolin, C., Patterson, M. A., Sanders, I., and Huntington, G. T. (2011). User's Manual for GPOPS Version 4.x: A MATLAB Software for Solving Multiple-Phase Optimal Control Problems Using hp-Adaptive Pseudospectral Methods. Report.

Rao, A. V., Benson, D. A., Darby, C., Patterson, M. A., Francolin, C., Sanders, I., and Huntington, G. T. (2010). Algorithm 902: GPOPS, a MATLAB software for solving multiple-phase optimal control problems using the Gauss pseudospectral method. *ACM Transactions on Mathematical Software (TOMS)*, 37(2):22:1–22:39.

Scheepmaker, G. M. and Goverde, R. M. P. (2015). The interplay between energy-efficient train control and scheduled running time supplements. *Journal of Rail Transport Planning & Management*, 5(4):225–239.

Scheepmaker, G. M. and Goverde, R. M. P. (2020). Energy-efficient train control using nonlinear bounded regenerative braking. *Transportation Research Part C: Emerging Technologies*, 121:102852.

Scheepmaker, G. M., Goverde, R. M. P., and Kroon, L. G. (2017). Review of energy-efficient train control and timetabling. *European Journal of Operational Research*, 257(2):355–376.

Scheepmaker, G. M., Pudney, P. J., Albrecht, A. R., Goverde, R. M. P., and Howlett, P. G. (2020a). Optimal running time supplement distribution in train schedules for energy-efficient train control. *Journal of Rail Transport Planning & Management*, 14:100180.

Scheepmaker, G. M., Willeboordse, H. Y., Hoogenraad, J. H., Luijt, R. S., and Goverde, R. M. P. (2020b). Comparing train driving strategies on multiple key performance indicators. *Journal of Rail Transport Planning & Management*, 13:100163.

Serafini, P. and Ukovich, W. (1989). A mathematical model for periodic scheduling problems. *SIAM Journal on Discrete Mathematics*, 2(4):550–581.

Sicre, C., Cucala, A. P., Fernández-Cardador, A., Jiménez, J. A., Ribera, I., and Serrano, A. (2010). A method to optimise train energy consumption combining manual energy efficient driving and scheduling. *WIT Transactions on The Built Environment*, 114:549–560.

Stephan, A. (2008). OpenPowerNet − Simulation of railway power supply systems. *WIT Transactions on The Built Environment*, 103:449–459.

Su, S., Li, L., Tang, T., and Gao, Z. (2013). A subway train timetable optimization approach based on energy-efficient operation strategy. *IEEE Transactions on Intelligent Transportation Systems*, 14(2):883–893.

Su, S., Tang, T., Li, X., and Gao, Z. (2014). Optimization of multitrain operations in a subway system. *IEEE Transactions on Intelligent Transportation Systems*, 15(2):673–684.

Su, S., Wang, X., Cao, Y., and Yin, J. (2020). An energy-efficient train operation approach by integrating the metro timetabling and eco-driving. *IEEE Transactions on Intelligent Transportation Systems*, 21(10):4252–4268.

UIC (2013). Uic code 406: Capacity. Report, UIC.

Vromans, M. J. C. M., Dekker, R., and Kroon, L. G. (2006). Reliability and heterogeneity of railway services. *European Journal of Operational Research*, 172(2):647–665.

Wang, P. and Goverde, R. M. P. (2016). Multiple-phase train trajectory optimization with signalling and operational constraints. *Transportation Research Part C: Emerging Technologies*, 69:255–275.

Wang, P. and Goverde, R. M. P. (2017). Multi-train trajectory optimization for energy efficiency and delay recovery on single-track railway lines. *Transportation Research Part B: Methodological*, 105:340–361.

Wang, P. and Goverde, R. M. P. (2019). Multi-train trajectory optimization for energy-efficient timetabling. *European Journal of Operational Research*, 272(2):621–635.

Xu, Y., Jia, B., Li, X., Li, M., and Ghiasi, A. (2020). An integrated micro-macro approach for high-speed railway energy-efficient timetabling problem. *Transportation Research Part C: Emerging Technologies*, 112:88–115.

Yan, F., Bešinović, N., and Goverde, R. M. P. (2019). Multi-objective periodic railway timetabling on dense heterogeneous railway corridors. *Transportation Research Part B: Methodological*, 125:52–75.

Yan, F. and Goverde, R. M. P. (2019). Combined line planning and train timetabling for strongly heteroge-

neous railway lines with direct connections. *Transportation Research Part B: Methodological*, 127:20–46.

Yang, L., Li, K., Gao, Z., and Li, X. (2012). Optimizing trains movement on a railway network. *Omega*, 40(5):619–633.

Yang, S., Wu, J., Yang, X., Sun, H., and Gao, Z. (2018). Energy-efficient timetable and speed profile optimization with multi-phase speed limits: Theoretical analysis and application. *Applied Mathematical Modelling*, 56:32–50.

Yang, X., Li, X., Ning, B., and Tang, T. (2016). A survey on energy-efficient train operation for urban rail transit. *IEEE Transactions on Intelligent Transportation Systems*, 17(1):2–13.

Yang, X., Ning, B., Li, X., and Tang, T. (2014). A two-objective timetable optimization model in subway systems. *IEEE Transactions on Intelligent Transportation Systems*, 15(5):1913–1921.

Yang, X., Wu, J., Sun, H., Gao, Z., Yin, H., and Qu, Y. (2019). Performance improvement of energy consumption, passenger time and robustness in metro systems: A multi-objective timetable optimization approach. *Computers & Industrial Engineering*, 137:106076.

Yin, J., Tang, T., Yang, L., Xun, J., Huang, Y., and Gao, Z. (2017). Research and development of automatic train operation for railway transportation systems: A survey. *Transportation Research Part C: Emerging Technologies*, 85:548–572.

Zhang, Y., D'Ariano, A., He, B., and Peng, Q. (2019). Microscopic optimization model and algorithm for integrating train timetabling and track maintenance task scheduling. *Transportation Research Part B: Methodological*, 127:237–278.

Zhou, Y., Bai, Y., Li, J., Mao, B., and Li, T. (2018). Integrated optimization on train control and timetable to minimize net energy consumption of metro lines. *Journal of Advanced Transportation*, 2018:19.

Appendices

A. Input case study

This appendix presents the input used for the case study. Table 6 shows the infrastructure data used for the case study in this paper with information about the gradients, speed limits and signal locations. The details about the rolling stock characteristics are shown in Table 7 and the timetable characteristics are visualized in Table 8.

Table 6: Infrastructure elements and related distance towards station Ah divided into block sections (ProRail, 2020). Legend: speed marker board indicates speed limit by multiplying the value by 10 (km/h), i.e., speed marker board 11 means speed limit of 110 km/h.

Infrastructure element	Distance from Ah (km)	Infrastructure element	Distance from Ah (km)
Station Ah & speed marker board 6 & gradient 0‰	0	Block signal 824	7.981
Entry/exit signal 2104 & speed marker board 8	0.420	Entry/exit signal A822	9.111
Speed marker board 11	0.906	Block signal 822	9.841
Entry/exit signal 2032	1.041	Station Est	10.309
Entry/exit signal 2014	1.621	Speed marker board 13	10.808
Gradient -11.6‰	1.866	Entry/exit signal 404	10.933
Gradient -5.9‰	1.882	Entry/exit signal 408	11.775
Gradient -4.4‰	2.045	Entry/exit signal 444	12.665
Gradient -6.1‰	2.353	Speed marker board 14	12.960
Gradient -2.25‰	2.711	Block signal 810	13.898
Block signal 834	2.807	Gradient 5.0‰	14.311
Gradient 0‰	2.911	Block signal 806	15.221
Speed marker board 14	2.973	Station Nml	16.054
Block signal 830	3.936	Speed marker board 11	16.336
Gradient -3.8‰	4.311	Entry/exit signal 166	16.521
Gradient -5.0‰	4.511	Speed marker board 4	17.656
Block signal 828	5.261	Gradient 0‰	17.211
Station Ahz	5.877	Entry/exit signal 162	17.791
Block signal 826	6.628	Station Nm	18.500
Gradient -2.5‰	6.811	Entry/exit signal 118	18.542
Gradient 0‰	7.211		

Table 7: Standard rolling stock characteristics (NS, 2020).

Rolling stock characteristic	IC	SPR
Rolling stock type	VIRM-1 XII	FLIRT-HRN IX
Number of coaches/wagons	12 (6+6)	9 (3+3+3)
Train length	324 m	189.6 m
Total train weight	782,000 kg	400,245 kg
Rotating mass factor	1.06	1.08
Maximum traction force	427.8 kN	387.0 kN
Maximum power	4,314.0 kW	4,407.0 kW
Maximum service braking deceleration	0.5 m/s^2	0.5 m/s^2
Traction efficiency	87.5%	90.6%
Maximum allowed speed	140 km/h	140 km/h
Train resistance equation:		
$r_0 + r_1\,v + r_2\,v^2$		
r_0	5,440.90 N	3,253.82 N
r_1	100.08 Ns/m	525.00 Ns/m
r_2	18.144 Ns^2/m^2	4.239 Ns^2/m^2

Table 8: Timetable characteristics and blocking time parameters.

Characteristic	Value
Gravitational acceleration g	9.81 m/s^2
Setup time interlocking area	12 s
Setup time open track	0 s
Driver sight and reaction time	9 s
Release time	2 s
Minimum dwell time SPR at intermediate stations	42 s
Minimum buffer time between two trains	30 s

B. Main results

This appendix presents the tables of the main results. Table 9 and Table 10 focus on the individual results of the IC and SPR train regarding the speed profile and running time supplement distribution. Table 9 shows the results of the different driving strategies of the IC and SPR by varying the running time supplements. The optimal running time supplement distribution for the SPR over the complete trajectory is shown in Table 10. Afterwards, the Tables 11–14 are focused on the results of the IC-SPR cycle. Table 11 shows the total running time per IC-SPR cycle for different running times for the IC and SPR. The extended cycle time for the IC-SPR cycles can be found in Table 12. The total buffer time for the different IC-SPR cycles is shown in Table 13. Finally, Table 14 shows the energy consumption of the different IC-SPR cycles.

Table 9: Results of the different driving strategies with varying running time supplements of the IC and SPR for the real-world case Ah-Nm.

Scenario	Figure	Trip time (s)	Running time supplements (%)	Energy consumption (kWh)	Energy saving (%)	N	Computation time (s)
Case Ah-Nm IC MTTC	4	643.1	0	456.2	0	200	36.8
Case Ah-Nm IC EETC 1%	4	649.6	1.0	346.9	24.0	200	53.0
Case Ah-Nm IC EETC 2%	4	656.0	2.0	313.2	31.3	200	34.4
Case Ah-Nm IC EETC 3%	4	662.4	3.0	286.9	37.1	200	28.0
Case Ah-Nm IC EETC 4%	4	668.9	4.0	274.1	39.9	200	29.6
Case Ah-Nm IC EETC 5%	4	675.3	5.0	264.3	42.1	200	50.9
Case Ah-Nm IC EETC 6%	4	681.7	6.0	255.7	44.0	200	56.2
Case Ah-Nm IC EETC 7%	4	688.2	7.0	246.4	46.0	200	48.2
Case Ah-Nm IC EETC 8%	4	694.6	8.0	238.9	47.6	200	47.7
Case Ah-Nm IC EETC 9%	4	701.0	9.0	232.4	49.1	200	36.0
Case Ah-Nm IC EETC 10%	4	707.4	10.0	227.0	50.2	200	61.0
Case Ah-Nm IC EETC 11%	4	713.9	11.0	219.5	51.9	200	30.0
Case Ah-Nm IC EETC 12%	4	720.3	12.0	212.4	53.4	200	81.5
Case Ah-Nm IC EETC 13%	4	726.7	13.0	208.4	54.3	200	43.8
Case Ah-Nm IC EETC 14%	4	733.1	14.0	202.6	55.6	200	83.5
Case Ah-Nm IC EETC 15%	4	739.6	15.0	196.9	56.8	200	27.7
Case Ah-Nm SPR MTTC	5	826.7	0	550.8	0	500	94.5
Case Ah-Nm SPR EETC 1%	5	834.9	1.0	449.7	18.4	600	238.4
Case Ah-Nm SPR EETC 2%	5	843.1	2.0	410.4	25.5	600	263.6
Case Ah-Nm SPR EETC 3%	5	851.4	3.0	381.9	30.7	600	262.0
Case Ah-Nm SPR EETC 4%	5	859.6	4.0	360.1	34.6	600	185.5
Case Ah-Nm SPR EETC 5%	5	867.9	5.0	341.1	38.1	600	323.3
Case Ah-Nm SPR EETC 6%	5	876.2	6.0	325.7	40.9	600	223.2
Case Ah-Nm SPR EETC 7%	5	884.5	7.0	312.2	43.3	600	171.9
Case Ah-Nm SPR EETC 8%	5	892.7	8.0	300.6	45.4	600	389.6
Case Ah-Nm SPR EETC 9%	5	901.0	9.0	291.0	47.2	650	311.4
Case Ah-Nm SPR EETC 10%	5	909.2	10.0	281.5	48.9	650	276.3
Case Ah-Nm SPR EETC 11%	5	917.5	11.0	273.4	50.4	670	325.2
Case Ah-Nm SPR EETC 12%	5	925.8	12.0	264.3	52.0	670	497.4
Case Ah-Nm SPR EETC 13%	5	934.1	13.0	256.6	53.4	670	348.7
Case Ah-Nm SPR EETC 14%	5	942.3	14.0	249.2	54.8	700	685.9
Case Ah-Nm SPR EETC 15%	5	950.6	15.0	242.4	56.0	700	471.3

Legend: N = number of collocation points, IC = Intercity, SPR = Sprinter, MTTC = minimum time train control, EETC = energy-efficient train control.

Table 10: Optimal running time supplement distribution for SPR for each section of the different real-world case Ah-Nm scenarios.

Scenario	RTS Ah–Ahz (s)	RTS Ahz–Est (s)	RTS Est–Nml (s)	RTS Nml–Nm (s)	RTS Ah–Nm (s)	Max. speed Ah–Ahz (km/h)	Max. speed Ahz–Est (km/h)	Max. speed Est–Nml (km/h)	Max. Nml–Nm (km/h)
Case Ah–Nm SPR MTTC	0.0 (0.0%)	0.0 (0.0%)	0.0 (0.0%)	0.0 (0.0%)	0.0 (0.0%)	140.0	140.0	140.0	101.5
Case Ah–Nm SPR EETC 1%	3.0 (1.2%)	2.2 (1.2%)	1.7 (0.8%)	1.3 (0.7%)	8.2 (1.0%)	126.3	134.4	140.0	91.2
Case Ah–Nm SPR EETC 2%	5.8 (2.3%)	4.6 (2.5%)	3.9 (1.8%)	2.2 (1.2%)	16.4 (2.0%)	119.6	129.2	135.9	88.1
Case Ah–Nm SPR EETC 3%	7.5 (3.0%)	7.3 (4.0%)	6.5 (3.0%)	3.4 (1.9%)	24.7 (3.0%)	116.9	124.3	131.8	85.2
Case Ah–Nm SPR EETC 4%	8.9 (3.6%)	10.2 (5.6%)	9.4 (4.3%)	4.5 (2.5%)	32.9 (4.0%)	114.4	120.5	130.0	83.3
Case Ah–Nm SPR EETC 5%	12.1 (4.9%)	12.7 (7.0%)	10.9 (5.0%)	5.4 (3.0%)	41.2 (5.0%)	110.0	117.5	130.0	81.4
Case Ah–Nm SPR EETC 6%	12.9 (5.2%)	15.9 (8.7%)	13.3 (6.2%)	7.4 (4.1%)	49.5 (6.0%)	110.0	114.4	128.7	78.8
Case Ah–Nm SPR EETC 7%	13.2 (5.3%)	18.9 (10.4%)	17.3 (8.0%)	8.4 (4.7%)	57.8 (7.0%)	110.0	111.2	125.6	77.4
Case Ah–Nm SPR EETC 8%	13.3 (5.3%)	22.4 (12.3%)	21.1 (9.7%)	9.3 (5.2%)	66.0 (8.0%)	110.0	108.0	122.9	76.3
Case Ah–Nm SPR EETC 9%	15.3 (6.1%)	24.5 (13.5%)	23.7 (11.0%)	10.8 (6.0%)	74.3 (9.0%)	108.5	106.5	121.4	74.6
Case Ah–Nm SPR EETC 10%	18.1 (7.3%)	26.6 (14.6%)	25.9 (12.0%)	11.9 (6.6%)	82.5 (10.0%)	106.3	104.6	120.0	73.5
Case Ah–Nm SPR EETC 11%	18.3 (7.4%)	27.6 (15.2%)	27.3 (12.6%)	17.6 (9.8%)	90.8 (11.0%)	106.0	103.9	119.2	69.0
Case Ah–Nm SPR EETC 12%	22.5 (9.0%)	30.7 (16.9%)	31.7 (14.7%)	14.2 (7.9%)	99.1 (12.0%)	102.6	101.8	116.9	71.7
Case Ah–Nm SPR EETC 13%	25.7 (10.3%)	33.3 (18.3%)	34.1 (15.8%)	14.3 (8.0%)	107.4 (13.0%)	100.6	100.0	115.6	71.7
Case Ah–Nm SPR EETC 14%	27.8 (11.2%)	35.6 (19.6%)	35.8 (16.6%)	16.3 (9.1%)	115.6 (14.0%)	99.1	98.4	114.7	70.1
Case Ah–Nm SPR EETC 15%	30.5 (12.2%)	37.9 (20.9%)	38.6 (17.9%)	16.9 (9.4%)	123.9 (15.0%)	97.6	97.1	113.4	69.5

Legend: RTS = running time supplement, Max. = maximum, IC = Intercity, SPR = Sprinter, MTTC = minimum time train control, EETC = energy-efficient train control, Ah = Arnhem Central, Ahz = Arnhem South, Est = Elst, Nml = Nijmegen Lent, Nm = Nijmegen.

Table 11: Total running time (s) per IC-SPR cycle for different running time supplements for the real-world case study Ah-Nm.

Running time supplements	IC 0%	IC 1%	IC 2%	IC 3%	IC 4%	IC 5%	IC 6%	IC 7%	IC 8%	IC 9%	IC 10%	IC 11%	IC 12%	IC 13%	IC 14%	IC 15%
SPR 0%	1469.8	1476.3	1482.7	1489.1	1495.6	1502.0	1508.4	1514.9	1521.3	1527.7	1534.1	1540.6	1547.0	1553.4	1559.8	1566.3
SPR 1%	1478.0	1484.4	1490.9	1497.3	1503.7	1510.1	1516.6	1523.0	1529.4	1535.9	1542.3	1548.7	1555.2	1561.6	1568.0	1574.5
SPR 2%	1486.3	1492.7	1499.1	1505.6	1512.0	1518.4	1524.8	1531.3	1537.7	1544.1	1550.6	1557.0	1563.4	1569.9	1576.2	1582.7
SPR 3%	1494.5	1500.9	1507.4	1513.8	1520.2	1526.7	1533.1	1539.5	1545.9	1552.4	1558.8	1565.2	1571.7	1578.1	1584.5	1591.0
SPR 4%	1502.8	1509.2	1515.6	1522.1	1528.5	1534.9	1541.4	1547.8	1554.2	1560.6	1567.1	1573.5	1579.9	1586.4	1592.7	1599.2
SPR 5%	1511.1	1517.5	1523.9	1530.4	1536.8	1543.2	1549.7	1556.1	1562.5	1569.0	1575.4	1581.8	1588.2	1594.7	1601.0	1607.5
SPR 6%	1519.3	1525.8	1532.2	1538.6	1545.1	1551.5	1557.9	1564.4	1570.8	1577.2	1583.7	1590.1	1596.5	1602.9	1609.3	1615.8
SPR 7%	1527.6	1534.0	1540.5	1546.9	1553.3	1559.7	1566.2	1572.6	1579.0	1585.5	1591.9	1598.3	1604.8	1611.2	1617.6	1624.1
SPR 8%	1535.9	1542.3	1548.7	1555.1	1561.6	1568.0	1574.4	1580.9	1587.3	1593.7	1600.2	1606.6	1613.0	1619.5	1625.8	1632.3
SPR 9%	1544.1	1550.6	1557.0	1563.4	1569.9	1576.3	1582.7	1589.2	1595.6	1602.0	1608.4	1614.9	1621.3	1627.7	1634.1	1640.6
SPR 10%	1552.4	1558.8	1565.2	1571.7	1578.1	1584.5	1591.0	1597.4	1603.8	1610.3	1616.7	1623.1	1629.6	1636.0	1642.3	1648.8
SPR 11%	1560.7	1567.1	1573.5	1579.9	1586.4	1592.8	1599.2	1605.7	1612.1	1618.5	1625.0	1631.4	1637.8	1644.3	1650.6	1657.1
SPR 12%	1568.9	1575.4	1581.8	1588.2	1594.7	1601.1	1607.5	1614.0	1620.4	1626.8	1633.2	1639.7	1646.1	1652.5	1658.9	1665.4
SPR 13%	1577.2	1583.6	1590.1	1596.5	1602.9	1609.4	1615.8	1622.2	1628.7	1635.1	1641.5	1647.9	1654.4	1660.8	1667.2	1673.7
SPR 14%	1585.4	1591.9	1598.3	1604.7	1611.2	1617.6	1624.0	1630.5	1636.9	1643.3	1649.8	1656.2	1662.6	1669.1	1675.4	1681.9
SPR 15%	1593.7	1600.2	1606.6	1613.0	1619.5	1625.9	1632.3	1638.7	1645.2	1651.6	1658.0	1664.5	1670.9	1677.3	1683.7	1690.2

Legend: IC = Intercity, SPR = Sprinter.

Table 12: Extended cycle time (s) per IC-SPR cycle for different running time supplements for the real-world case study Ah-Nm.

Running time supplements	IC 0%	IC 1%	IC 2%	IC 3%	IC 4%	IC 5%	IC 6%	IC 7%	IC 8%	IC 9%	IC 10%	IC 11%	IC 12%	IC 13%	IC 14%	IC 15%
SPR 0%	670.8	666.1	662.5	659.8	656.8	652.8	648.9	644.5	640.3	635.8	631.9	627.0	622.2	618.4	614.3	609.8
SPR 1%	698.3	693.7	690.9	687.3	684.3	680.4	676.4	671.9	667.9	664.0	660.2	654.5	650.0	645.8	641.7	637.3
SPR 2%	706.5	701.9	699.2	695.6	692.5	688.6	684.7	680.1	676.1	672.2	668.4	662.8	658.3	654.0	649.9	645.6
SPR 3%	714.8	710.2	707.5	703.8	700.8	696.9	692.9	688.4	684.4	680.5	676.7	671.0	666.5	662.3	658.2	653.8
SPR 4%	723.0	718.4	715.7	712.1	709.0	705.1	701.2	696.6	692.6	688.7	684.9	679.3	674.8	670.5	666.4	662.1
SPR 5%	731.3	726.7	724.0	720.3	717.3	713.4	709.4	704.9	700.9	697.0	693.2	687.5	683.0	678.8	674.7	670.3
SPR 6%	739.5	734.9	732.2	728.6	725.5	721.6	717.7	713.2	709.2	705.2	701.5	695.8	691.3	687.0	682.9	678.6
SPR 7%	747.8	743.2	740.5	736.8	733.8	729.9	725.9	721.4	717.4	713.5	709.7	704.0	699.5	695.3	691.2	686.8
SPR 8%	756.0	751.5	748.7	745.1	742.0	738.2	734.2	729.7	725.7	721.8	718.0	712.3	707.8	703.5	699.5	695.1
SPR 9%	764.3	759.7	757.0	753.4	750.3	746.4	742.5	737.9	733.9	730.0	726.2	720.6	716.1	711.8	707.7	703.3
SPR 10%	772.6	768.0	765.3	761.6	758.6	754.7	750.7	746.2	742.2	738.3	734.5	728.8	724.3	720.1	716.0	711.6
SPR 11%	780.7	776.1	773.4	769.8	766.7	762.8	758.9	754.4	750.4	746.4	742.7	737.0	732.5	728.2	724.2	719.8
SPR 12%	789.1	784.5	781.8	778.1	775.1	771.2	767.2	762.7	758.7	754.8	751.0	745.3	740.8	736.6	732.5	728.1
SPR 13%	797.3	792.7	790.0	786.4	783.3	779.4	775.5	770.9	766.9	763.0	759.2	753.6	749.1	744.8	740.7	736.4
SPR 14%	805.6	801.0	798.3	794.6	791.6	787.7	783.7	779.2	775.2	771.3	767.5	761.8	757.3	753.1	749.0	744.6
SPR 15%	813.8	809.2	806.5	802.9	799.8	795.9	792.0	787.5	783.5	779.5	775.8	770.1	765.6	761.3	757.3	752.9

Legend: IC = Intercity, SPR = Sprinter.

EJTIR 21(4), 2021, pp.1-42
Scheepmaker and Goverde
Multi-objective railway timetabling including energy-efficient train trajectory optimization

41

Table 13: Total buffer time (s) including the minimum buffer time (60 s) per IC-SPR cycle for different running time supplements for the real-world case study Ah-Nm. Note that the drop in the buffer time is caused by the frequency increase of the IC-SPR cycle (from 4 to 5 trains per hour).

Running time supplements	IC 0%	IC 1%	IC 2%	IC 3%	IC 4%	IC 5%	IC 6%	IC 7%	IC 8%	IC 9%	IC 10%	IC 11%	IC 12%	IC 13%	IC 14%	IC 15%
SPR 0%	109.2	113.9	117.5	120.2	123.2	127.2	131.1	135.5	139.7	144.2	148.1	153.0	157.8	161.6	165.7	170.2
SPR 1%	81.7	86.3	89.1	92.7	95.7	99.6	103.6	108.1	112.1	116.0	119.8	125.5	130.0	134.2	138.3	142.7
SPR 2%	73.5	78.1	80.8	84.4	87.5	91.4	95.3	99.9	103.9	107.8	111.6	117.2	121.7	126.0	130.1	134.4
SPR 3%	65.2	69.8	72.5	76.2	79.2	83.1	87.1	91.6	95.6	99.5	103.3	109.0	113.5	117.7	121.8	126.2
SPR 4%	237.0	61.6	64.3	67.9	71.0	74.9	78.8	83.4	87.4	91.3	95.1	100.7	105.2	109.5	113.6	117.9
SPR 5%	228.7	233.3	236.0	239.7	62.7	66.6	70.6	75.1	79.1	83.0	86.8	92.5	97.0	101.2	105.3	109.7
SPR 6%	220.5	225.1	227.8	231.4	234.5	238.4	62.3	66.8	70.8	74.8	78.5	84.2	88.7	93.0	97.1	101.4
SPR 7%	212.2	216.8	219.5	223.2	226.2	230.1	234.1	238.6	62.6	66.5	70.3	76.0	80.5	84.7	88.8	93.2
SPR 8%	204.0	208.5	211.3	214.9	218.0	221.8	225.8	230.3	224.3	238.2	62.0	67.7	72.2	76.5	80.5	84.9
SPR 9%	195.7	200.3	203.0	206.6	209.7	213.6	217.5	222.1	226.1	230.0	233.8	239.4	63.9	68.2	72.3	76.7
SPR 10%	187.4	192.0	194.7	198.4	201.4	205.3	209.3	213.8	217.8	221.7	225.5	231.2	235.7	239.9	64.0	68.4
SPR 11%	179.3	183.9	186.6	190.2	193.3	197.2	201.1	205.6	209.6	213.6	217.3	223.0	227.5	231.8	235.8	60.2
SPR 12%	170.9	175.5	178.2	181.9	184.9	188.8	192.8	197.3	201.3	205.2	209.0	214.7	219.2	223.4	227.5	231.9
SPR 13%	162.7	167.3	170.0	173.6	176.7	180.6	184.5	189.1	193.1	197.0	200.8	206.4	210.9	215.2	219.3	223.6
SPR 14%	154.4	159.0	161.7	165.4	168.4	172.3	176.3	180.8	184.8	188.7	192.5	198.2	202.7	206.9	211.0	215.4
SPR 15%	146.2	150.8	153.5	157.1	160.2	164.1	168.0	172.5	176.5	180.5	184.2	189.9	194.4	198.7	202.7	207.1

Legend: IC = Intercity, SPR = Sprinter.

Table 14: Total traction energy consumption (kWh) per IC-SPR cycle for different running time supplements for the real-world case study Ah-Nm.

Running time supplements	IC 0%	IC 1%	IC 2%	IC 3%	IC 4%	IC 5%	IC 6%	IC 7%	IC 8%	IC 9%	IC 10%	IC 11%	IC 12%	IC 13%	IC 14%	IC 15%
SPR 0%	1007.0	897.7	864.1	837.8	825.0	815.2	806.5	797.2	789.8	783.2	777.8	770.4	763.2	759.3	753.4	747.7
SPR 1%	905.9	796.6	763.0	736.7	723.9	714.1	705.4	696.1	688.6	682.1	676.7	669.3	662.1	658.1	652.3	646.6
SPR 2%	866.6	757.3	723.7	697.4	684.6	674.8	666.1	656.8	649.4	642.8	637.4	630.0	622.8	618.9	613.0	607.3
SPR 3%	838.1	728.8	695.1	668.8	656.0	646.2	637.6	628.3	620.8	614.3	608.9	601.4	594.3	590.3	584.4	578.8
SPR 4%	816.3	706.9	673.3	647.0	634.2	624.4	615.7	604.4	599.0	592.4	587.0	579.6	572.4	568.5	562.6	556.9
SPR 5%	797.3	687.9	654.3	628.0	615.2	605.4	596.7	587.4	580.0	573.4	568.0	560.6	553.4	549.5	543.6	536.9
SPR 6%	781.9	672.6	638.9	612.6	599.8	590.0	581.3	572.1	564.6	558.1	552.6	545.2	538.1	534.1	528.2	522.5
SPR 7%	768.4	659.1	625.5	599.2	586.4	576.6	567.9	558.6	551.2	544.6	539.2	531.8	524.6	520.7	514.8	509.1
SPR 8%	756.8	647.4	613.8	587.5	574.7	564.9	556.2	547.0	539.5	532.9	527.5	520.1	513.0	509.0	503.1	497.4
SPR 9%	747.2	637.9	604.3	578.0	565.2	555.4	546.7	537.4	529.9	523.4	518.0	510.6	503.4	499.4	493.6	487.9
SPR 10%	737.7	628.4	594.7	568.4	555.6	545.8	537.1	527.9	520.4	513.9	508.4	501.0	493.9	489.9	484.0	478.4
SPR 11%	729.6	620.3	586.7	560.4	547.5	537.8	529.1	519.8	512.3	505.8	500.4	493.0	485.8	481.8	476.0	470.3
SPR 12%	720.5	611.2	577.5	551.2	538.4	528.6	520.0	510.7	503.2	496.7	491.3	483.8	476.7	472.7	466.9	461.2
SPR 13%	712.8	603.4	569.8	543.5	530.7	520.9	512.2	502.9	495.5	488.9	483.5	483.5	470.4	466.5	460.6	460.6
SPR 14%	705.4	596.1	562.4	536.1	523.3	513.5	504.9	495.6	488.1	481.6	476.2	468.7	461.6	457.6	451.8	446.1
SPR 15%	698.6	589.3	555.6	529.3	516.5	506.7	498.1	488.8	481.3	474.8	469.3	461.9	454.8	450.8	444.9	439.3

Legend: IC = Intercity, SPR = Sprinter.